UNIVERSIDADE DA BEIRA INTERIOR
Engenharia

Preliminary Topology Optimization of Small Unmanned Aircraft Wings for Additive Manufacturing

Cátia Alexandra Louro Miguel

Dissertação para obtenção do Grau de Mestre em

Engenharia Aeronáutica

(ciclo de estudos integrado)

Orientador: Prof. Doutor Pedro Vieira Gamboa

Covilhã, fevereiro de 2019

“A person who never made a mistake never tried anything new.”

Albert Einstein

Acknowledgements

I would like to thank all the people that accompanied me through this journey and made me a better person.

First, I would like to thank my supervisor Pedro Vieira Gamboa, for all the guidance, support and patience throughout this work. His motivation was essential for the accomplishment of the work.

Secondly to Pedro Alves and Pedro Carneiro for the advice and help through this work.

I would also thank my friends who, over these years, shared with me good moments and I will always keep with me. Thank you to André, António, Bruna, Cátia, Daniel, Flávia, Francisco, Gabriel, Inês, João Miguel, João Rocha, Luís Coelho, Luís Oliveira, Mara, Nicole, Nídia, Nuno, Pedro and Rodolfo.

Lastly, I would like to thank the most important people in my life, my parents. Without them, nothing would be possible, and I am grateful for all they have done for me. Thank you for all the love and courage you gave me!

Resumo

O Fabrico Aditivo (FA) descreve os processos que criam peças em 3D, sendo estas fabricadas camada-por-camada. A tecnologia do FA já abrange, hoje em dia, uma grande variedade de materiais, não havendo essa barreira quando é proposto um projeto. Permite também a produção de mais peças em menos tempo, o que faz com que haja uma redução de custos e de desperdício de material. A Otimização Topológica combina o método dos elementos finitos com fórmulas matemáticas de otimização, proporcionando assim uma melhor distribuição de material no domínio de referência da geometria em análise. Esta otimização pode ser aplicada de modo a melhorar o desempenho de produtos já existentes ou para criar novos. Ao juntar estas duas ferramentas, o FA com a otimização topológica, é possível criar estruturas mais leves, com maior rigidez e complexidade. O que antigamente não era fazível, devido à limitação nos moldes e ferramentas nos métodos tradicionais.

Esta dissertação procura a possibilidade de usar a otimização topológica como ferramenta para obter uma asa, para um avião não tripulado (UAV), mais leve. O objetivo é investigar as características de rigidez e resistência de uma asa, sendo apresentados diferentes casos para análise. O trabalho descreve os designs e os procedimentos numéricos, em que se enquadram a dinâmica dos fluidos computacional, as análises estruturais e a otimização topológica. A otimização foi realizada com o objetivo de minimizar a massa. Todo o procedimento numérico foi efetuado no software ANSYS.

Ao realizar este trabalho, houve um caso de estudo que se destacou apresentando uma redução de 74% da massa, ainda assim para os requerimentos da aeronave em questão são necessários mais estudos.

Palavras-chave

Asa, Fabrico Aditivo, Otimização Topológica

Abstract

Additive Manufacturing (AM) describes the processes which produce 3D parts, being these manufactured through a layer-by-layer procedure. The AM technology takes a wide variety of materials, so there is not a barrier in that field when a project is proposed. It also allows the part production in less time, reducing the costs and material waste. Topology Optimization combines the finite element method with mathematical optimization formulas, providing a better material distribution in the reference domain of the geometry under analysis. This optimization can be applied to improve the performance of existing products or to create new ones. By combining these two tools, AM and topology optimization, create lighter structures with greater rigidity and complexity is possible. Which previously was not possible due to the limitation in tools and molds of traditional methods.

This work searches the possibility of using topology optimization as a tool to obtain a lighter wing to an unmanned aerial vehicle (UAV). The objective is to investigate the stiffness and strength characteristics of a wing, being presented in different cases for analysis. This dissertation describes the designs and numerical procedures, in which are included computation fluid dynamics, structural analysis, and topology optimization. The optimization was realized with the aim of minimizing mass. The entire numerical procedure was performed in ANSYS software.

In this work, there is a study case which was evidencing, due to the 74% of weight reduction, but for the aircraft requirements in the study, more investigations are necessary, since the final design wing has, approximately, 1.5kg and the UAV should have a mass of 5kg.

Keywords

Wing, Additive Manufacturing, Topology Optimization

Content

List of Figures

List of Tables

Nomenclature

b	Filter factor	[-]
B	Bulk modulus	[Pa]
C	Constant	[-]
$C_{1\varepsilon}$	Constant	[-]
$C_{2\varepsilon}$	Constant	[-]
C_{μ}	Constant	[-]
C_L	Lift coefficient	[-]
C_m	Constitutive matrix	[Pa]
E	Elastic Modulus	[Pa]
E_0	Elastic matrix of initial solid element	[Pa]
E_i	Elastic matrix	[Pa]
F	External force vector	[N]
G	Shear Modulus	[Pa]
h	Volume ratio	[-]
H	Sensitivity filter	[-]
k	Turbulent kinetic energy	[m^2/s^2]
K	Global stiffness matrix	[Pa]
L	Lift	[N]
L_{al}	Adjoint load vector	[N]
N	Total number of discrete numbers	[-]
p	Penalization	[-]
r_{filter}	Mesh filter radius	[m]
S	Wing area	[m^2]
S_{ut}	Ultimate tensile strength	[Pa]
u	Displacement vector	[m]
U	Global displacement vector	[m]
X	Design variable vector	[-]
$\bar{v}_i$	Element volume after optimization	[m^3]
V	Velocity	[m/s]
V_0	Initial volume	[m^3]
V_{ad}	Adjoint displacement vector	[m]
w_j	Weight function	[kg]
x_i	Position of element i	[m]
x_j	Position of element j	[m]
x_t	Ultimate longitudinal tensile strength	[MPa]
y_t	Ultimate transverse tensile strength	[MPa]

Greek symbols

ε	Strain	[-]
ε_d	Dissipation rate	[m^2/s^2]
σ	Stress	[Pa]
σ_ε	Constant (Turbulent Prandtl number for dissipation rate)	[-]
σ_k	Constant (Turbulent Prandtl number for kinetic energy)	[-]
σ_y	Yield Strength	[Pa]
σ_{lim}	Yield stress limit	[Pa]
σ_{vm}	Von Mises stress	[Pa]
ρ	Density	[kg/m^3]
ρ_i	Element i density	[kg/m^3]
$\widetilde{\rho_\iota}$	Filtered i density	[kg/m^3]
ρ_j	Element j density	[kg/m^3]
ρ_{min}	Minimum limit of element relative density	[kg/m^3]
μ	Dynamic Viscosity	[kg/(m.s)]
v	Poisson’s ration	[-]
Ω	Reference domain	[m^3]

Acronyms

3D	Three Dimensional
ABS	Acrylonitrile Butadiene Styrene
AM	Additive Manufacturing
ANSYS	Analysis of Systems
BC	Boundary Condition
CAD	Computer-Aided Design
FDM	Fused Deposition Modelling
FEA	Finite Element Analysis
FEM	Finite Element Method
FGM	Functionally Graded Materials
PLA	Polylactic Acid
SIMP	Solid Isotropic Material with Penalization
TO	Topology Optimization
UAV	Unmanned Aerial Vehicle
UBI	Universidade da Beira Interior

Chapter 1

Introduction

1.1 Motivation

Nowadays, parts are possible to manufacture through Additive Manufacturing (AM) technology, more specifically 3D printing, which consists of a print of a three-dimensional model generated using a CAD system, created by successive layers of material [1]. The original name for 3D printing was rapid prototyping because a product could be rapidly and automatically created without any complexity [2]. The term AM was given by the committee (F42) of American Society for Testing and Materials (ASTM), in 2009 [2]. Since then, multiple new technologies using different materials, including metallic, ceramic and polymeric materials, became commercially available [3]. AM technology has been studied due to its advantages because it can be used to remove or simplify many of multi-stage processes, reducing time when compared to traditional methods. AM process is illustrated in Figure 1.1.

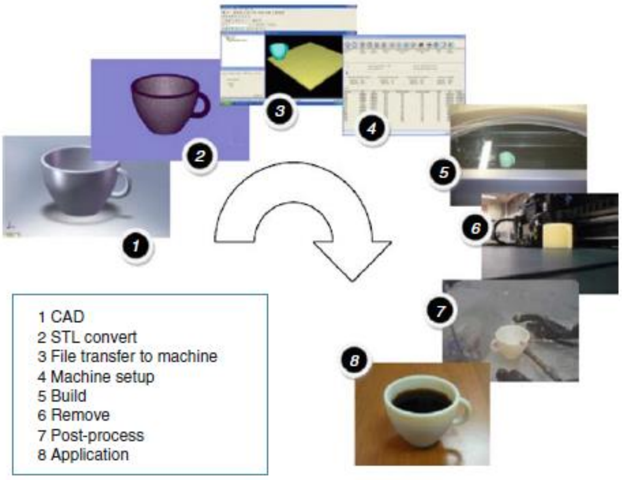

Figure 1.1 – Generic process of CAD to part [4].

AM can be combined with Topology Optimization (TO), which is a numerical method that enables the weight optimization of any geometry complying with previously requirements.

These new methods and technologies allow the reduction of using parts that leads to fewer critical failures. Considering these implications, safer aircrafts could be produced, and many lives could be saved. Thus, the need to continue the development of these tools is crucial.

1.2 Objectives

The purpose of this dissertation is to investigate the possibility of using TO in the design of a small unmanned aerial vehicle (UAV) wing that is to be produced by an additive manufacturing technology. For that, the following tasks were defined:

- Design geometry in CATIA V5 for implementation on CFD analysis;
- Structural analysis in ANSYS for different design geometries, applying the boundaries conditions and the results from CFD analysis;
- Topology optimization of previous designs, with the intention of weight reduction.

1.3 Dissertation Outline

This dissertation is divided into 5 chapters. The first and current chapter includes motivation and objectives.

The second chapter is dedicated to the literature review, where the technologies of AM are presented, as well as, the advantages and disadvantages, including the materials used. Some printing cases of UAVs and parts of its are also presented. TO is presented at the end of this chapter, emphasizing the Solid Isotropic Material with Penalization (SIMP) method, where the formulas behind the method are shown.

The numerical methods are described in the third chapter. Firstly, the software used is described. Then, the numerical setup is presented, where it is divided into 4 sub-sections. The first sub-section is a brief presentation of ANSYS Workbench. The second is dedicated to Fluent, where the used model, mesh and boundary conditions (BCs) are being described. The third includes the mechanical study, where the material's properties are presented, and an explanation of the setup. The fourth is dedicated to topology optimization.

The fourth chapter refers to the study cases and the results from mechanical and topology optimization.

The fifth and final chapter reports the conclusions and possible future works for this topic.

Chapter 2

Literature Review

2.1 Additive Manufacturing

2.1.1 Definition

In 2012, ASTM defined AM technology as capable of “joining materials to make objects from 3D model data” [1]. The initial purpose of the technology was to create prototypes, for all sectors, in a flexible and fast manner [2].

AM involves processes based on continuous deposition of material, layer-by-layer until a physical object is created without labor resources, following instructions from a computer with a virtual model designed in a CAD system. In these processes, metal, polymers, or ceramics materials are used, through highly specialized machines [2]. For each of these technologies, there are at least two materials: the production material and the support material. The support is, in most of the cases, cleaned and becomes a manufacturing residue [5]. With the evolution of materials and processes, AM became a natural tool to solve some specific problems for small series direct production (rapid manufacturing), tooling production and more recently a powerful tool to produce cost-effectively complex parts. Nowadays, faster and cheaper AM techniques have been developed with high print quality. Polymer materials for 3D printing are being produced with a wider range of properties [6].

These technologies are revolutionizing the world of manufacturing, bringing forward the so-called *Fourth Industrial Revolution (4.0 Industry)*, where the production processes tend to become increasingly efficient, autonomous and customizable [3].

2.1.2 Processes

The commercial AM most used are:

1. Stereolithography (SLA)

SLA was the first commercially available process in 1986. Initially, there were only a few materials that could be used, however, with today advancements, there is a greater variety.

The basic concept of stereolithography is photocurable resin printing, typically acrylic or epoxy, by exposing it to ultraviolet (UV) light of a specific wavelength, and then the exposed 2D-patterned resin layers become solid through a process called photopolymerization [1, 2, 6].

2. Fused Deposition Modelling (FDM)

It is one of the most used techniques which uses a spool of a thermoplastic filament with varying diameters to be melted and extruded through a heated nozzle. The materials used are nylon, Acrylonitrile Butadiene Styrene (ABS), Polylactic Acid (PLA) and aerospace grade Ultem^{TM}. This technique is based on automatic deposition of filament material and a filament of support one. T5his process is repeated layer-by-layer, until the physical model is finished, as illustrated in Figure 2.1. In the end, the support material is taken out through a process like ultra-sound bath. Recently, thermoplastics with higher melting temperatures such as PEEK can already be used as materials for desktop 3D printing, which are the most popular consumer-level polymer composites 3D printers.

As long as the errors are below the accuracy level of the machine process ($\approx 0.5\text{mm}$), they are acceptable. The machine's language is STL and then it prints one layer (2D) on top of the other, forming at the end a 3D object [2, 6, 7, 8].

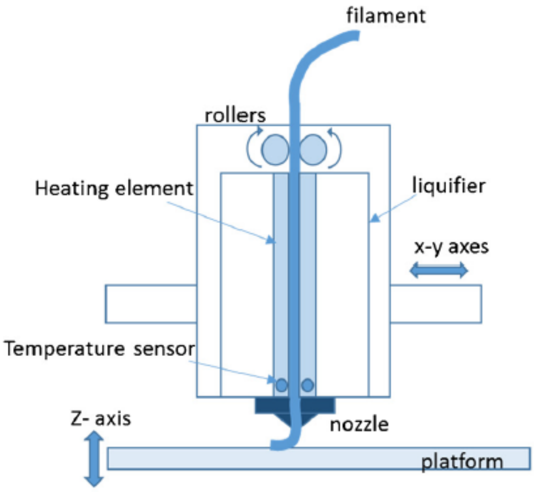

Figure 2.1 – Schematic of fused deposition molding (FDM) process [8].

3. Selective Laser Sintering (SLS)

It is a process where a laser beam transfers energy into a surface containing a thin layer of pre-heated powder material. The energy transferred by the laser beam fuses specific areas of the surface. After fusing one layer, another one is deposited and again the laser fuses this layer that will bind in the previous one [2].

4. Multi Jet Modelling (MJM) or Polyjet

It is a process where a print head containing hundreds of nozzles selectively spreads in a surface a photopolymeric material that is cured by the incidence of a specific wavelength. Another print head spreads support material, normally in form of a gel that is also polymerized. It is a continuous process where the platform is reduced to a tenth of a millimetre for each layer. In the end, the support material is removed through a water jet [2].

5. 3D Printing (3DP)

It was developed by the Massachusetts Institute of Technology (MIT) and, today is one of the most popular because of the low costs of acquisition and operation. It is a type similar to SLS where a multi-nozzle print head selectively spreads a liquid binder in a platform with a powder. The binder reacts with the powder to compose a layer while the platform is moved down. The process repeats until the end of the part. The quality of the final product depends on powder particle size, the viscosity of the binder, binder-powder interaction, and the speed of the binder deposition [2, 6].

2.1.3 Advantages and Disadvantages

Advantages:

- *Energy optimization*: According to the USA Energy Department, AM can reduce energy costs by 50% and material costs by 90%. The design and fabrication processes have been reduced from weeks to a few hours [2, 6].
- *Reduction in material waste:* It is supposed that with AM, the only material required is the one used to create parts. However, it is not completely true because sacrifice support structures sometimes are necessary and some materials, special polymers, degrades with continuous use under heating [2].
- *Special tooling and speed:* There is great flexibility to produce many different parts at the same time, without the necessity of special tooling or equipment. AM systems are capable to manufacture 3D components and products directly from raw materials and 3D design data [1, 2].
- *Design optimization:* It is possible to produce complex shapes, so our mind is the limitation [1, 6].
- Possibility to create low quantities of products, or just one, providing the absence of cost relating to tools, as well as, reducing the number of parts in inventory since could be produced on-site [1].
- Producing parts neglecting the prototype development phase. A direct translation of design to component [3, 7].
- Different size ranges could be printed, from micro to several meters sized parts [2].

Disadvantages:

- Slow process speed [1].
- Poor dimensional accuracy compared to some conventional processes [1].
- Rough surface finish and problems with process repeatability [1].
- The inherent anisotropic property of the printed parts. A result of AM techniques is that the microstructure of the materials would tend to grow in a certain direction causing different mechanical property along the layer. Consequently, parts manufactured through additive processes show a preferential bearing direction, normally the one along which the material is deposited [8, 9].
- AM is more economical when total build volume is lesser than 130 units, below that injection moulding should be used. Additional processes are needed to make the material into the forms that are suitable for AM processes, that is why material costs are higher than conventional techniques [8].

2.2 Materials

The materials types used in AM processes have a large range, including metallic, ceramic and polymeric materials along with combinations in the form of composites, hybrid or functionally graded materials (FGM) [3]. Each process (mentioned in 2.1.2) requires different materials [8]. Mechanical properties of AM parts can be affected by unprinted materials and the technique used. Nowadays, there are no standard tests for mechanical characterization because of the undefined mechanical behaviour of 3D printed parts, and this happens for two reasons. Firstly, because of the high number of parameters to control during the process. Secondly because of the high anisotropy, which is defined by their manufacturing history, as the resistance of the raw material and the cohesive forces between bonded layers [6]. Dizon et al. (2017) [6] concluded that 3D-printed materials have large anisotropy, especially for the FDM and SLS printed parts. The AM aim is to print a part with excellent quality with minimal anisotropy.

Between these materials, polymers have been mostly used perhaps due to their widespread use in the first-generation rapid prototyping machines [3]. Polymers have relatively lower melting and glass transition temperatures, which make it easier to flow at a relatively lower temperature than ceramics and metals. Bonding involving metals and ceramics are not easy to achieve, as it is with polymers due to their high melting temperatures. Normally, plastics have lower strength than metals, however, they have lower density and higher strains at failure. There are some cases that plastics will have higher strength, per unit weight, than metals [10]. In many cases are added special fillers as carbon nanotubes, graphene, nanocellulose, nanoclay or nano silica to improve polymers performance [3], just like it happens with the project of Zhang et al. [8]. They print the frame, tail, and gears for flapping wing UAV using ABS copolymers material, after all, they found that using only ABS was not sufficient to provide the required strength, and then they reinforced the parts with carbon fibre rods and polyester films for better strength.

Relatively to the characterization of powder materials and final products, Caputo et al. [11] made a study. Since the processes of AM involve heat exchange phenomena, must be taken into account the knowledge of the thermal behaviour of starting powder materials. Another important aspect is their density and porosity. Porosity is a property that strongly affects the quality of parts and for the measure of this feature there are ultrasonic non-destructive testing, Archimedes method or micro X-ray computed tomography. Advanced image processing techniques are useful in the AM environment to develop better quality control and reliability. Non-destructive characterization methodologies allow to detect failures and to describe the structure. They concluded that measuring the properties of powders is mandatory for the industry to select proper raw materials.

2.2.1 Polymers

Polymers are macromolecules formed through smaller structural unities. They have structures much more complex than metals or ceramics parts and they can be easily processed. Nevertheless, they have low relative strength, elasticity module and operating temperature limits.

Polymers are subdivided into two classes: thermoplastics and thermosetting. A thermoset is a material that cures into a given shape, generally through the application of heat (curing is an irreversible chemical reaction in which permanent connections are made between the material's molecular chains). A thermoplastic is a polymer that shapes with the application of heat,i.e. its viscosity becomes smaller on heating. Cooling to room temperature makes the strongest thermoplastics [10].

2.2.1.1 Polylactic Acid (PLA)

The most frequent source materials for commercially-available FDM printers are ABS and PLA. Bulk PLA characteristics can be seen in Table 2.1.

Table 2.1 – Material properties of bulk PLA [12].

Material property	Units	Value
Density (ρ)	kg/m^3	1240
Elastic modulus (E)	Pa	3500×10^6
Shear modulus (G)	Pa	1287×10^6
Poisson's ratio (ν)	-	0.36
Yield strength (σ_y)	Pa	70×10^6
Ultimate tensile strength (S_{ut})	Pa	73×10^6
Elongation	%	~7

Industrial and general use of PLA is increasing due to the fact of its biocompatibility with the environment, and for this reason, now many desktop consumer printer models use, exclusively, PLA.

Torres et al. (2015) [12] present a study where they tested torsion of PLA materials resulting from FDM and the effects of processing parameters including layer thickness, percent infill, and post-processing via heat treatment. They concluded that heat treatment can cause an increase in strength, especially in low-infill components. But this increase in strength provides a loss in ductility.

Some studies have recently reported the tensile strength of different polymers, as summarized in Table 2.2.

Table 2.2 – Ultimate tensile strength (MPa) of different thermoplastics 3D-printed by FDM [13].

Raster Angle	ABS	Polypropylene	Polycarbonate	PLA	PEI
90º	26	32	19	54	40
0º	34	36	59.7	58	59
Authors	Rezayat et al.	Carneiro et al.	Hill et at.	Letcher et al.	Bagsik et al.

These studies revealed that PLA has a better mechanical response than the other thermoplastics polymers, and in tensile strength plane these materials are anisotropic, with the strength along the direction of extrusion (0º) exceeding that in the transverse direction (90º). Research by Ahn et al. [13] showed that the printing orientation and air gap had the most significant impact on the mechanical properties of the printed objects; but on the other side, the printing orientation and the platform temperature have a significant impact on structural inhomogeneity.

Y. Song et al. (2017) [13] quantify anisotropy and asymmetry of the mechanical response of PLA parts produced by FDM. The elastic material response was transversely isotropic for 3D-printed specimens and isotropic for injection-moulded specimens. They study specimens of porosity of order 1% and conclude that the porosity of 3D-printed material can be minimised by optimising the temperature and speed of extrusion, as well as, the speed of the printing head. Manufacturing by 3D-printing increases the crystallinity of the material, reducing its ductility and increasing the fracture toughness. The elastic response of 3D-printed material is transversely isotropic, although the anisotropy is smooth. They proved that 3D-printing does not affect material elasticity because both axial and transverse stiffness are similar to the one in injection-moulded PLA and the inelastic response of the material is ductile and orthotropic. They conclude that 3D printed PLA is tougher than injection-moulded PLA, due to the layered and filamentous nature of 3D-printed material and the complexity that this induces in the microscopic mechanisms of fracture. These experiments showed that in compression the material stiffness was nearly independent of axial strain, indicating a response governed solely by plasticity, with negligible damage. In contrast, in tension the material stiffness decreased as a function of strain, indicating the presence of damage mechanisms in conjunction with material's plasticity.

2.3 Printing Cases of Unmanned Aerial Vehicles (UAVs)

Unmanned aerial vehicles are gaining popularity due to their application in military, private and public sector, especially where human operator is not required. Evolution of UAVs started during World War II and it has come a long way for all operations, military and non-military. Birds and insects are the inspiration for some UAV's designs and the most desired are the light-weight UAVs due to a better performance in terms of shorter take-off range and longer flight endurance. When operating at low Reynolds number the performance largely depends upon a complex combination of specific and precisely orientated geometrical forms, for example, flapping wing UAV has several potential benefits over fixed wings, as a better manoeuvring, low speed, landing, and vertical take-off. Although a UAV design is specific to its mission requirements, having high endurance is something that all have in common [8]. Table 2.3 summarizes the classification of UAVs as defined by UVS International.

Table 2.3 – Classification of UAVs as defined by UVS International [8].

UAV category	Range [km]	Flight altitude [m]	Endurance [hours]	Max. take-off weight [kg]
Micro	<10	250	1	<5
Mini	<10	150-300	<2	<30
Medium range	70-200	5000	6-10	1250
Medium altitude long endurance	>500	14000	24-48	1500
High altitude long endurance	>2000	20000	24-48	12000

Recent research on cellular structures and topology optimization have resulted in complex light-weight UAV structures that cannot be fabricated using conventional manufacturing techniques, so AM presents itself as a better option because there is no design limit [8]. Table 2.4 shows which AM technology was used for a UAV component or even an entire UAV.

Table 2.4 – Name of UAVs or printed parts for each type of AM technique [8].

Types of AM techniques	Name of UAVs/ printed parts
FDM	Fully printed; AMRC UAV; VAST UAV; Frame, gear, tail
Polyjet	Lattice structure; Wing strut; Ornithopter; Replica of insect wing
SLA	Entomopter; Stingray UAV; Flap; Wind tunnel; UAV model
SLS	SULSA UAV; Scaled-down UAV; tunnel test; Spotter UAV

2.3.1 FDM printed Fixed Wing UAV – AMRC UAV

During the built process of FDM is necessary a broad number of support material in order to prevent deformation, and this adds a direct material cost and significantly increases built time. In 2014, a prototype UAV was design, manufacture and flight test by a team of engineers from AMRC's (Advanced Manufacturing Research Centre) new Design & Prototyping Group (DPG), entirely of ABS plastic (ABS-M30), using FDM technology. For printing large components, such the airframe, FDM was chosen, took less than 24 hours, which would be unthinkable because before of AM optimization, the airframe would take 120 hours to produce. The UAV showed good stability, and low aerodynamic noise at speed indicated an efficient wing design [14].

2.3.2 RecordRotor

In 2015, Altair Engineering in cooperation with Politecnico di Torino developed components for a structure of a multi-rotor, named RecordRotor. The challenge was to interface arms, consisting of carbon fibre tubes, with motor or frame, in 7075 Alloy. They use topology optimization to minimize the weight and additive manufactured polymer components played an important role in the prototype which was designed at the upper boundary of the normative with an MTOW of 25kg. They demonstrate that with a scientific methodology and with the support of innovative design tools was possible to construct high-performance components for the aerospace industry, with optimization included [7].

2.3.3 SULSA UAV

Figure 2.2 – SULSA [15].

SULSA (Southampton University Laser Sintered Aircraft) was the first 'printed' aircraft. Professors Andy Keane and Jim Scanlan from the University's Computational Engineering and Design Research group led the project. Kean's team set out how quickly they could design a 1.5-metre wingspan, super-low-drag UAV, print it and get it airborne. The plane parts took two days to design and five days to print, making this UAV a one-week plane. The constraints in the project were that they needed the use of a launch catapult and a belly landing because there was no undercarriage to keep complexity and weight down [15, 16].

2.3.4 World’s First Jet-Powered, 3D-Printed UAV

Aurora Flight Science and Stratasys Ltd developed a 3D-printed, jet-powered UAV with the ability to reach speeds up to 241 km/h. It has a wingspan of 3m and weighs only 15kg, as illustrated in Figure 2.3. 80% of the UAV was created using FDM process and the fuselage was made of nylon and the engine exhaust duct was 3D-printed in metal [17].

Figure 2.3 – Aurora Flight Sciences’ high-speed UAV is 80 percent 3D-printed with Stratasys’ additive manufacturing solutions [17].

2.3.5 EASYMAX 001

EASYMAX 001 has a wingspan of 1527mm, as presented in Figure 2.4. It is easily printed and possible to buy it, with a cost of 20$ and with an instruction manual included. Even the wing and the fuselage have a 3D structure reinforcement, which makes the UAV very rigid while maintaining a lightweight, even when it is made only from polymers [18].

Figure 2.4 – EASYMAX 001 [18].

2.3.6 University of Manito7gba – Team Kinect12

In 2011, the Composites Innovation Centre (CIC) requested Team Kinect12, from the University of Manitoba, to develop a manufacturing process for a small airplane wing, which utilizes rapid prototyping. The objectives that the client established was that the wing should weight no more than 0.45kg and must structurally be capable of lift and support a 2.3kg UAV. The process should also avoid the traditional methods of UAV wing construction and should be applicable to other structures.

The final wing design, of Team Kinect12, consists of RP frame modules, carbon fibre veneers, webs, and a spar. The veneers are adhered to the exterior shell to provide torsional strength for the wing and additionally provide the surface of the aerofoil, as represented in Figure 2.5 and Figure 2.6. The spar is to provide high specific strength and covers the entire span of the wing at 25% of the chord. The frame is produced in nine different modules, printed in ABS [19]. Figure 2.7 illustrates the final geometry that was printed through rapid prototyping.

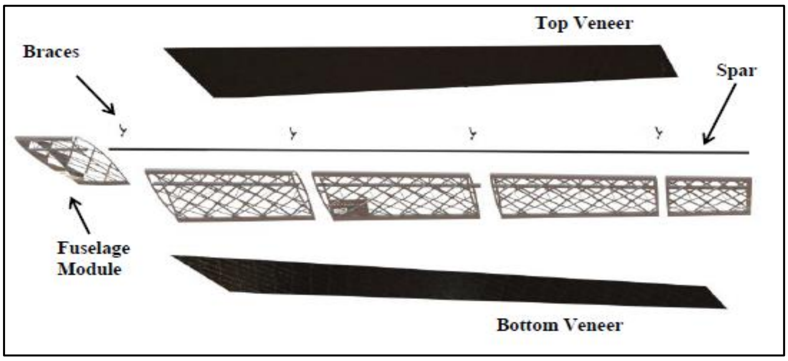

Figure 2.5 – View of one half of the wing assembly [19].

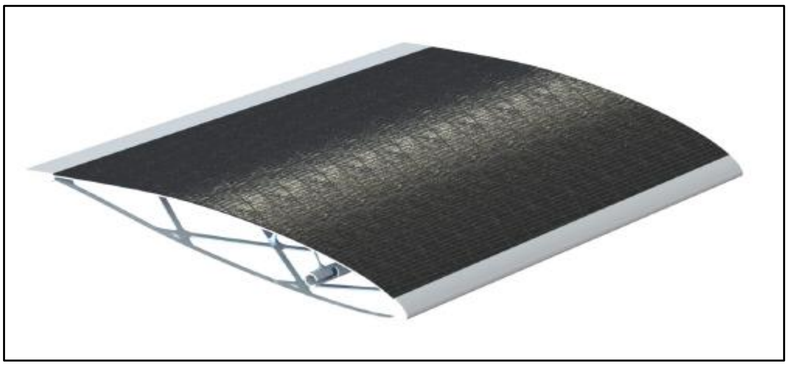

Figure 2.6 – Carbon-fibre veneer adhered to frame module, making up the wing surface [19].

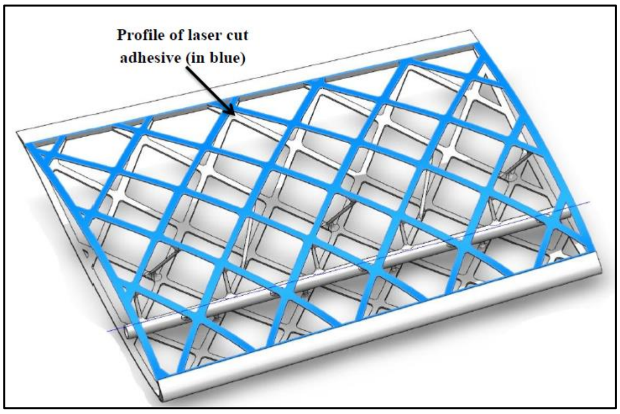

Figure 2.7 – Final geometry that was printed [19].

The team's setback was that RP machine had a lower resolution than some of the details provided in CAD models, so these details were not printed, and thus were not included in final geometry. But still, they were able to accomplish all the requirements established by CIC.

2.3.7 Air Force Institute of Technology

Walker et al. (2015) [20] decided to join AM with TO with the objective of creating a complex wing structure. The TO objective was minimizing compliance, which means maximizing the stiffness. They decided to apply the optimized wing in a UAV due to the relaxed airworthiness requirements. The final objective of their work was focused only on the main wing body structure, disregarding internal components like fuel tank, electronics, and cables. The wing structure had two small structural constraints near the centre of the design space. All the analysis was conducted considering only the skin of the wing, spars, and ribs. The wing was structurally constrained at the wing root and aerodynamic forces were applied for defined conditions.

For TO, the wing skin was considered a non-design space. The design space, the region where the optimization occurred, was the wing interior. And in the centre of design space, there were two small structural constraints, which belongs to non-design space (the region where optimization does not occur). The optimization constraint used was to maintain a volume fraction of the overall design space of less than 30 percent and the material used by them was an aluminum alloy. Figure 2.8 shows the initial design after the optimization and shows the structure after TO.

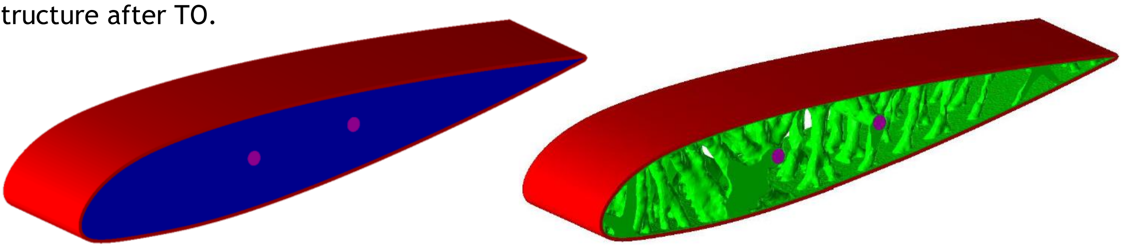

Figure 2.8 – Initial design space for TO, where blue corresponds to design space and red and pink corresponds to non-design space, presented at left. Topology optimized is illustrated at right [20].

Figure 2.9 presented the 3D printed wing, which was the purpose of the work.

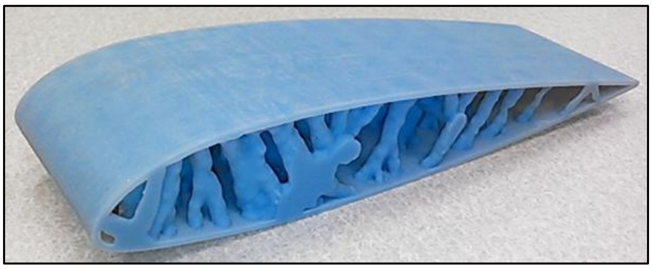

Figure 2.9 – 3D printed wing [20].

Figure 2.10 is representing the timeline of the evolution of AM's processes and development of UAVs.

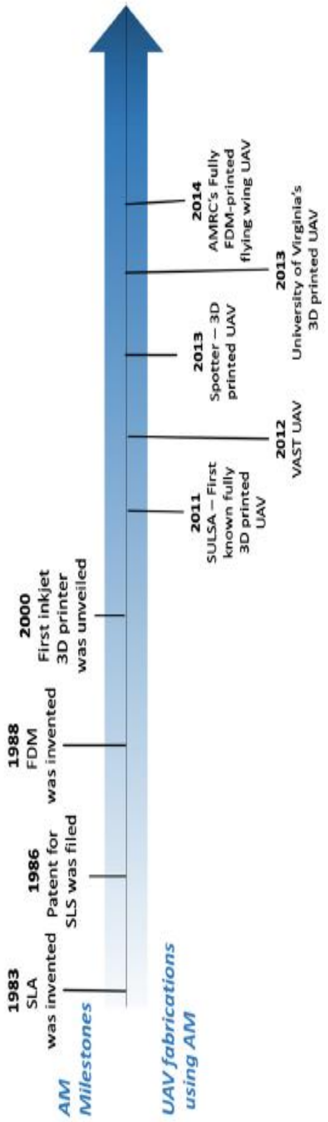

Figure 2.10 – Timeline representing development of AM processes and UAV fabrications using AM [8].

2.4 Structural Optimization

A continuum structure, relatively to the structural optimization, can be divided into Shape Optimization, Size Optimization and TO, as illustrated in Figure 2.11. Compared to the first two optimizations, TO can change the structure of the part, achieving designs that are not greatly constrained by the nature of the initial design [21, 22]. TO matches Finite Element Method (FEM) with mathematical formulas of optimization, with the aim of providing the best material distribution [23].

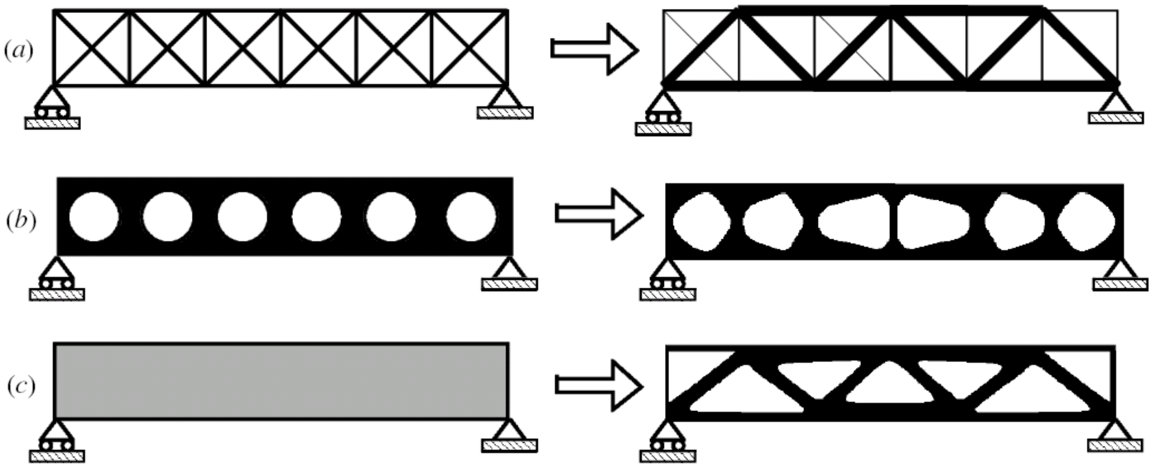

Figure 2.11 – Three different structural optimization types. a) Size; b) Shape; c) Topology [24].

2.4.1 Finite Element Method

The FEM is a mathematical approach in which to solve a problem it subdivides into smaller elements that keep the same properties compared to the initial. Differential equations are used to describe these elements and are solved by mathematical models to obtain results with more accuracy, but only gives an approximate solution [25, 26]. Several Finite Element (FE) based methods have been developed for topology optimization of continuum structures. The Finite Element Analysis (FEA) method, originally introduced by Turner et al. (1956) [27], is a powerful computational technique for approximate solutions to a variety engineering problems, having complex domains subjected to general BCs. It has become an essential step in the design or modelling of a physical phenomenon. This physical phenomenon occurs in a continuum domain involving several variables and the field of variables vary from element point to point, possessing an infinite number of solutions in the domain. FEA reduces the problem to a finite number dividing the domain into elements and expressing the unknown field variable in terms of the assumed approximating functions within each element. These functions are defined by the nodes, and these nodes are usually located along the element boundaries, and they connect adjacent elements [28, 29].

2.4.2 Topology Optimization

The coupling between AM and TO provides innovations forms, which with traditional manufacturing could be impossible to turn them into a part, but with additive manufacturing it is conceivable, and it can be applied in plastics, metals, etc. [5]. Over the last decade, TO has appeared as one of the numerous optimization techniques being used by most aircraft manufacturers due to its capability to generate light-weight conceptual designs [30]. The purpose of this optimization is to find the optimal layout within a specified region, knowing the support conditions, the applied loads and the volume constraints, being unknown the shape, the physical size and the connectivity of the structure [31]. TO has important practical applications by the manufacturing (i.e. car and aerospace) industries and has a significant role in micro and nanotechnologies [28].

In 1977, Prager and Rozvany [28] formulated the first general theory of topology optimization. Many optimization methods such as homogenization technique (Bendsøe and Kikuchi 1988 [28]), solid isotropic material with penalization (SIMP) (Bendsøe 1989; Zhou and Rozvany 1991 [28]) and evolutionary structural optimization (ESO) (Xie and Steven 1993, 1997 [28]) have been developed. SIMP, that was developed in the late eighties, and BESO is the most widely used algorithms, owing to their efficiency and simplicity [22, 32]. BESO (bi-directional ESO) is the latest version of ESO. It is a combination of additive evolutionary structural optimization (AESO) and ESO. In this method, the wasteful material is removed while efficient material is added to the structure, at the same time. However, BESO is limited to the TO of an objective function such as mean compliance with a single constraint, as structural volume [28, 29, 33]. SIMP will be discussed later in subchapter 2.4.3 since will be the method used in this dissertation.

As previously presented AM materials are constituted by production material and the support one and this optimization can match both, as exemplified in Figure 2.12.

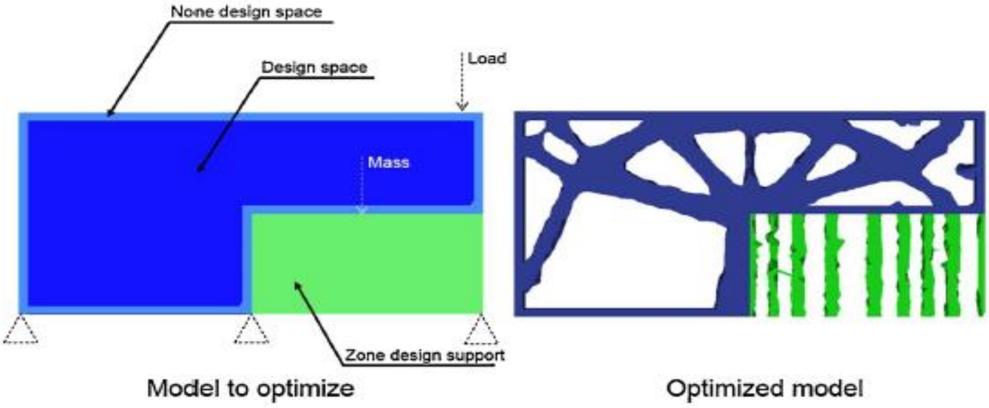

Figure 2.12 – Example of a topological optimization [5].

TO problem can be defined as the search for the best allocation or distribution of material in a given design space. The reference domain Ω (Ω Є R^3) is determined by the design space, loads and BCs. The design space corresponds to the interior of the objects and a non-design space corresponds to the skin of the object [5].

About existing topological optimization models, these can be divided according to the type of topology involved. Taking in consideration that the first term corresponds to the base material and the second to the type of elements, there are four large groups being designated as Isotropic-Solid (IS), Isotropic-Solid/Empty (ISE), Anisotropic-Solid/Empty (ASE) and Isotropic-Solid/Empty/Porous (ISEP) (includes Isotropic-Solid/Empty/Composite (ISEC) and Isotropic-Solid/Empty/Composite-Porous (ISECP)) [30]. For simplicity, the ISE and IS topologies are specified in this work. Within the models ISE and IS there are used the following strategies: Solid Isotropic Microstructures with Penalization (SIMP), Optimal Microstructures with Penalization (OMP), NonOptimal Microstructures (NOM) and Dual Discrete Programming (DDP). Below explained the strategies in Table 2.5:

Table 2.5 – Methods used for large ISE or IS topologies in generalized shape optimization [32].

	SIMP	**OMP**	**NOM**	**DDP**
Microstructure of elements	Solid, isotropic	Optimal nonhomogeneous	Nonoptimal nonhomogeneous	Solid, isotropic
Additional penalization	Yes	Yes	No	Not necessary
Homogenization necessary	No	Yes	Yes	No
Number of free parameters	1	2D:3ou 4 3D:5 ou 6	>1	1
Available for:	All combinations of design constraints	Compliance	All combinations of design constraints	Compliance
Penalization adequate	Yes	Yes	No	-

SIMP as becoming generally accepted in topology optimization as a technique of considerable advantages.

2.4.3 SIMP: Solid Isotropic Material with Penalization

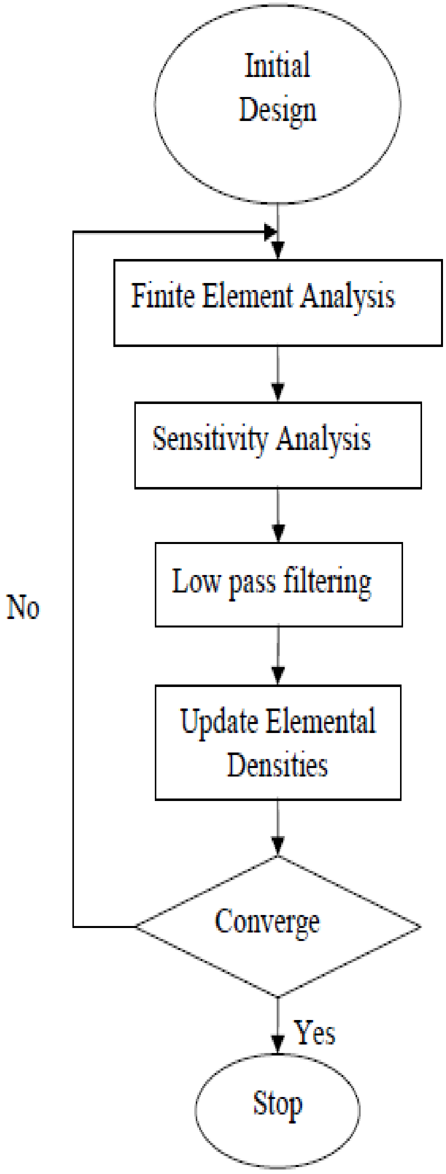

Figure 2.13 - SIMP flow chart [22].

The term “SIMP” is sometimes called “material interpolation”, “power law”, “artificial material” or “density” method [28]. The basic idea of this method is discretizing the design domain by finite element mesh and optimize the density variables associated to each element within the discretization, as represented in Figure 2.13 [33]. The design variables are a series of material densities, which are denoted by $\rho_i \in [0,1]$. Each node in the finite element mesh has its own density variable, ρ_i, and the element shape functions are used to construct a continuous density field. Regions where $\rho \approx 0$ are interpreted as being void of material, while regions where $\rho=1$ are interpreted as being solid, because intermediate density values are just a mathematical tool for representing non-physical stated, the SIMP formulation penalizes intermediate densities using an exponential penalty function and the results will depend on the degree of penalization [30]. The relationship of elastic matrix *Ei*, the effective Young's modulus, and element density ρ_i in optimization process can be written as

$$E_i = \rho_i^p E_0 \quad (2.1)$$

where p is a penalization value and E_0 elastic matrix of the initial solid element [34]. For $p=1$, the problem corresponds to the classical 'variable thickness sheet optimization' which is studied by Cheng and Olhoff and lots of grey density elements $0<\rho_i<1$ which have no physical meaning are obtained. Choosing p too low or too high either causes too much grey scales or too fast convergence to local minima, and lots of numerical examples show that $p=3$ ensures good convergence to almost 0-1 solutions [33].

SIMP is used in practice for highly complex non-convex problems and most commercial TO software have implemented SIMP for TO, being ANSYS one of them [22, 28].

Chapter 3

Numerical Methods

3.1 Software description

Nowadays, technology allows the numerical study without experimental tests, giving the opportunity to realize studies that in an experimental way have a high cost. In this chapter, it will be discussed the software used, in a succinct way.

3.1.1 ANSYS

ANSYS is the original name for commercial products. The company develops a complete range of CAE (Computer Aided Engineering) products. It is a general-purpose finite-element modelling package for numerically solving a wide variety of mechanical problems. These problems include static/dynamic, structural analysis (both linear and nonlinear), heat transfer, and fluid problems, as well as acoustic and electromagnetic problems [35].

3.1.1.1 Workbench

ANSYS Workbench helps drive all of the simulations in a single environment. The platform guides the user through complex multiphysics analyses with drag and drops simplicity, providing bi-directional CAD connectivity [36]. ANSYS Workbench is often used in conjunction with CAD software such as DesignModeler or SpaceClaim.

3.1.1.2 Fluent

ANSYS Fluent provides comprehensive modelling capabilities for a wide range of incompressible and compressible, laminar and turbulent fluid flow problems. Steady-state and transient problems can be performed. In this type of analyse a broad range of mathematical models for transport phenomena is combined with the ability to model complex geometries. A very useful group of models in Fluent is the set of free surface and multiphase flow models, therefore, can be used for analysis of gas-liquid, gas-solid, liquid-solid and gas-liquid-solid flows. Accurate and robust models are a vital component of Fluent suite of models [37].

3.1.1.3 Mechanical

Mechanical is a module in ANSYS to set up and run structural analyses. Topology optimization was introduced in 2018 with ANSYS 18.0, integrating its own solver and pre and post-processing tools [24].

3.1.1.4 SpaceClaim/DesignModeler

SpaceClaim and DesignModeler are CAD software integrated into several modules of ANSYS. SpaceClaim is the most recent and more upset to topology optimization because it can read STL files exported from Mechanical and post-process the geometry before design validation. The geometry is converted then into a solid for ANSYS Mechanical to analyse again as validation process.

3.1.2 CATIA

It is a multi-platform software suite for CAD, computer-aided manufacturing (CAM), CAE developed by the French company Dassault Systèmes.

3.1.3 XFLR5

XFLR5 is an analysis tool for aerofoils, wings, and planes operating at low Reynolds Numbers.

3.2 Numerical Setup

In this chapter, the numerical methods and the numerical setup will be presented. Firstly, ANSYS Workbench will be explained. The second section is dedicated to ANSYS Fluent, describing the flow properties, that uses various convergence schemes to equate the flow properties along the boundaries and the principal aim of this section is to calculate lift, drag and pressure distribution along the wing. In this section mesh quality and model, setup is described. The third section corresponds to the Mechanical part and material data is provided, the mesh quality and the steps that have been taken in setup, in a general way, because there is be given more emphasis of this part in the next chapter. The fourth section refers to the topology optimization, including the design and exclusion regions, and the objective of the problem. Figure 3.1 illustrates the overall procedure, for better comprehension.

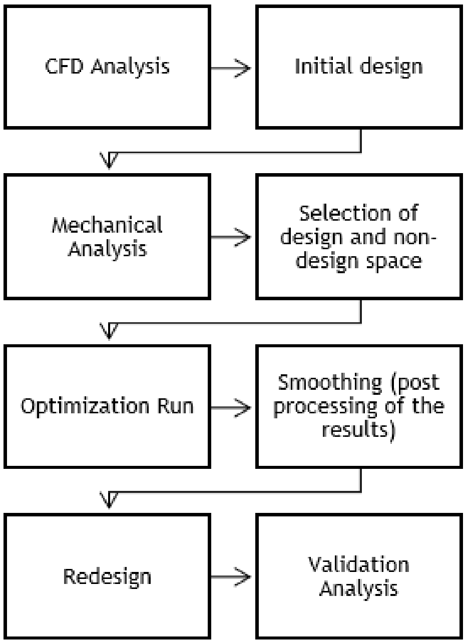

Figure 3.1 – Introduction to the overall procedure.

3.2.1 Analysis setup

Figure 3.2 shows a typical setup in ANSYS Workbench. Firstly, an analysis is made in Fluent, in order to determine the wing's pressure distribution. Then, after the meshing is done in Static Structural and the loads are applied, the topology optimization can be initiated with the results from the two-previous analysis. The last analysis in Mechanical is to validate the design.

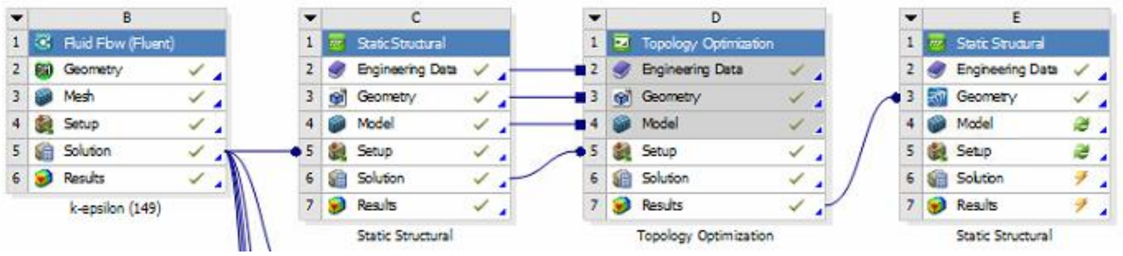

Figure 3.2 – ANSYS Workbench.

3.2.2 Fluent

Wing structures have a significant role because they are responsible to create lift. In movement, pressure distribution around the aerodynamic surface is created, which translates into the aerodynamic force. Fluent is used to determine the pressure distribution around the wing surface, in this dissertation.

3.2.2.1 Mesh

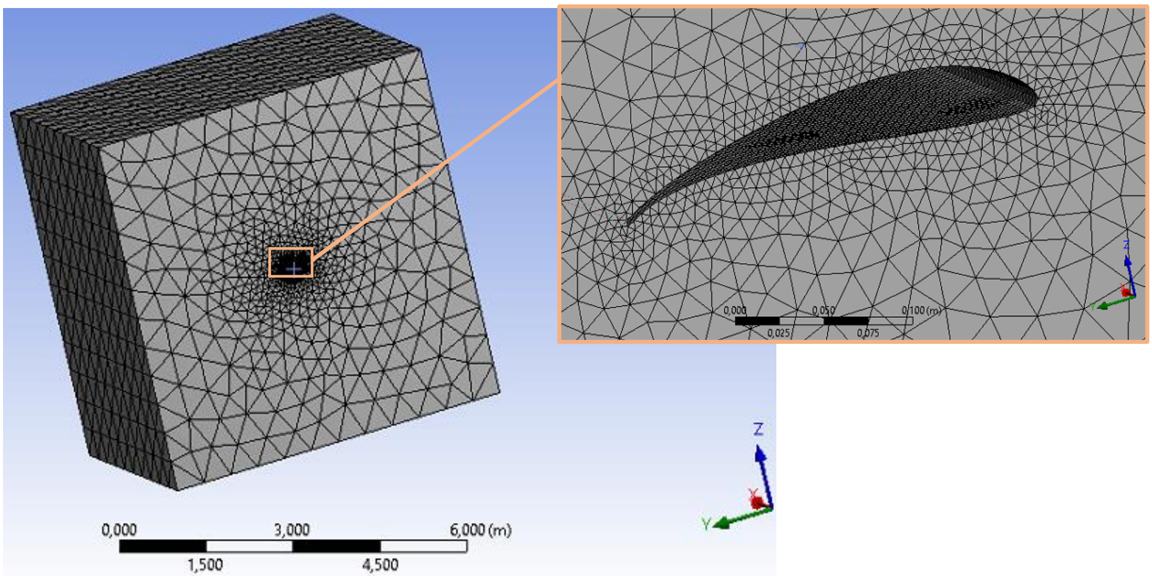

Figure 3.3 – Mesh around the aerofoil.

Figure 3.3 shows the geometry mesh, giving more focus to the wing surface. The mesh is obtained due to parameters that ANSYS provide, being generated automatically, and in this case, have 102571 nodes and 562983 elements. For flow analysis, the mesh should be defined between the aerofoil walls and the boundaries. These boundaries the further away from the aerofoil, better, meanwhile for this type of analysis the ambient conditions are used to define the BCs. In this study the boundaries are in a distance 20 times bigger than the aerofoil chord, to make results more accurate.

In this Fluent's section, it is possible to view the orthogonal quality, through mesh metric. This parameter is to ascertain the mesh quality, providing a scale between 0 and 1, and the closer to 1 the better the element. This metric is based on the following scale, as it is represented in Table 3.1:

Table 3.1 – Orthogonal Quality mesh metrics spectrum [38].

Unacceptable	Bad	Acceptable	Good	Very good	Excellent
0-0.001	0.001-0.14	0.15-0.20	0.20-0.69	0.70-0.95	0.95-1.00

Figure 3.4 and Table 3.2 show the number of elements within each quality range. Based on Table 3.1, it is verified that 0.09% of the elements are below acceptable.

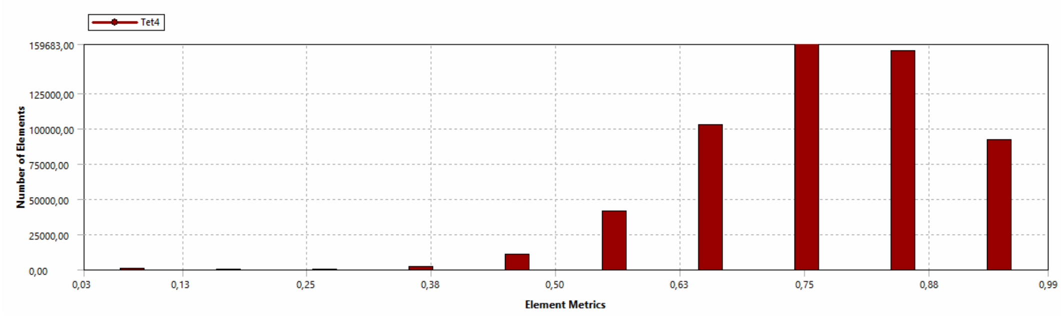

Figure 3.4 – Representation of element quality in ANSYS Fluent.

Table 3.2 – Correspondence of percent of the number of elements with the classification of orthogonal quality, a mesh metric from ANSYS Fluent.

Classification	Percent of number of elements
Unacceptable	0%
Bad	0.09%
Acceptable	0.004%
Good	18.874%
Very Good	75.135%
Excellent	5.897%

The BCs must be assigned to the faces of the control volume. In the present case, three types of BCs are used: symmetry, inlet, and outlet. The symmetry condition is applied to the face that contains the root of the wing because, since symmetric flight conditions are to be analysed, only half of the wing needs to be simulated. The inlet conditions are applied to the face upstream of the wing. The outlet conditions are applied to the face downstream of the wing, the face upper and down. Figure 3.5a) and Figure 3.5b) exemplifies the faces where the BCs are applied, where A corresponds to symmetry, B is the inlet and C, D, E and F the outlet.

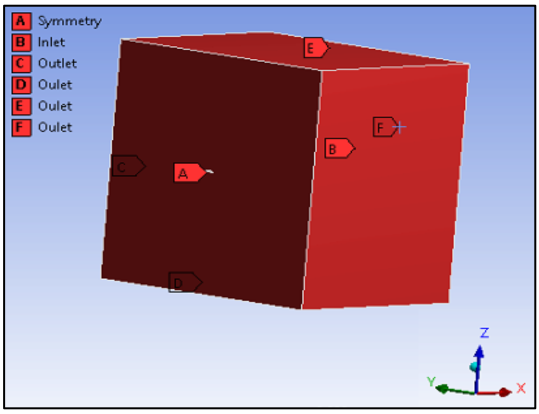

Figure 3.5a) – Domain boundaries definition, focus in symmetry and outlet.

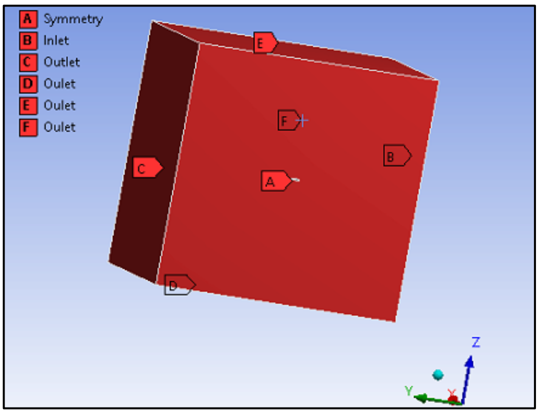

Figure 3.5b) – Domain boundaries definition, focus in symmetry and inlet.

3.2.2.2 Setup

The solver chosen was the pressure-based solver, since it is suitable in incompressible and mildly compressible flows. The velocity formulation chosen was absolute because it is preferable in applications where the flow in most of the domain is not rotating. The steady-state simulation was chosen due to its easier convergence as there are fewer terms to model.

After computing solutions with different turbulent models such as, k-omega SST model and transition k-kl-omega (3 eqn), the standard k-epsilon (ε) turbulent model is used since its results presented are more similar to the ones that result from XFLR5, relatively to L and C_L. This model is commonly used, and it was developed by Jones and Launder and has been modified by other investigators. It gained popularity in industrial flow owed to its economy, toughness, and reasonable accuracy for a wide range of turbulence flows. K-ε model is based on model transport equations for the turbulence kinetic energy (k) and its dissipation rate (ε_d), assuming that the flow is fully turbulent, and the effects of molecular viscosity are negligible. $C_{1\varepsilon}$, $C_{2\varepsilon,}$ and C_μ are constants that have the following values: 1.44, 1.92 and 0.09, respectively. σ_k is the turbulent Prandtl number for k, which has the value of 1.0 and σ_ε is the turbulent Prandtl number for ε, which is equal to 1.3. These values have been determined from experiments for fundamental turbulent flows and they work well for a wide range of wall-bounded and free shear flows.

The fluid used is air with the following properties: $\rho=1.225kg/m^3$ and $\mu=1.7894\times10^{-5}kg/(m.s)$. As mentioned in subsection 5.2.2.1, the BCs were applied on the faces. The inlet, referred to as face B in Figure 3.6b), corresponds to the Velocity Inlet, and these data are in functions of velocity, its magnitude, and direction. The direction of the velocity, in component y and z, was based on the angle of attack to the most critical flight condition, which for this UAV was 11°, according to the preliminary results obtained in XFLR5 for a Reynolds number of 3.94×10^5. The results obtained in XFLR5 were based in an analysis, with speed fixed of 24m/s, based on the method of horseshoe vortex (VLM1). As explained in section 3.1, XFLR5 is an analysis tool for wings operating at low Reynolds numbers, and for this reason, this software was used, as a way of comparison with the results obtained in Fluent. According to Table A.1, from the Appendix A, for a maximum take-off weight of 150N, the angle of attack corresponding is, approximately, 11°, so, for this reason, the chosen angle was this, as it was previously said. The correspond C_L for this condition is 1.765. These parameters were obtained through the following lift formula:

$$L = \frac{1}{2}\rho C_L V^2 S \quad (3.1)$$

where L represents lift, C_L is the lift coefficient, V is the velocity of the aircraft, ρ is the air density, which changes due to altitude, and S is the wing area. The lift must be equal to the aircraft's weight.

The output data was the Pressure Outlet (letter C, in Figure 3.6a)), which allows defining an outlet pressure differential equal to zero, allowing the flow to develop freely and in it's entirely within the control volume.

3.2.3 Mechanical

In general, a finite-element solution may be broken into three stages:

- Preprocessing - defining the problem: the key points, areas, lines, volumes, the element type and material/geometrical properties and mesh.
- Solution – Assigning loads, constraints and solving.
- Postprocessing – further processing and viewing of the results [35].

In this section, the parameters that are evaluated corresponds to equivalent (von-Mises) stress, total deformation, and strain energy. But for this evaluation, first, the materials to be used throughout the work are characterized. Then, the mathematical formulas of the parameters are established below, both for isotropic materials, in this work is PLA, and for orthotropic materials, which is the case of fibre carbon.

To obtain an accurate result is necessary, then, to create a mesh in the structure, under study. A mesh is composed of elements and nodes. The structure is divided by elements, and these elements are connected by nodes. After the resulting mesh, it is necessary to apply the BCs, so that the software does the static analysis.

For all the geometries analysed in Mechanical and TO, the axis system is the same. The x-axis, where occurs the wingspan variation, has an interval from 0 to 1m, when x is equal to zero corresponds to wing root and when x is equal to 1m corresponds to wing tip. The y-axis positive describes the chord variation, and the interval varies between 0 to 0.25m. Finally, the z-axis corresponds to the wing height. Figure 3.6 exemplify the axis system.

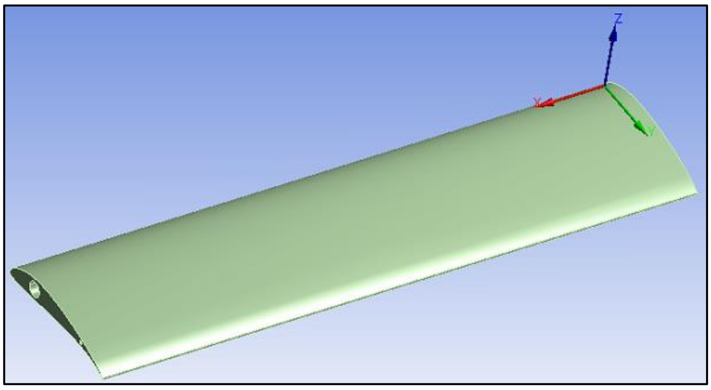

Figure 3.6 – Axis system illustration.

3.2.3.1 Engineering Data

Two materials are used in this work, polylactic acid (PLA) and unidirectional carbon fibre reinforced plastic (CFRP). The properties of these materials are summarized in Table 3.3.

Table 3.3 – Properties of unidirectional carbon fibre reinforced plastics and PLA [39, 40].

Orthotropic Material		**Isotropic Material**	
UD-CFRP		PLA	
Density [kg/m^3]	1600	Density [kg/m^3]	1240
E_x [MPa]	121×10^3		
E_y [MPa]	7.46×10^3	E [MPa]	3500
E_z [MPa]	7.46×10^3		
v_{xy}	0.31	v	0.36
v_{yz}	0.44		
v_{xz}	0.31	G [MPa]	1.29×10^9
G_{xy} [MPa]	5.18×10^3		
G_{yz} [MPa]	2.59×10^3	B [MPa]	4.17×10^9
G_{xz} [MPa]	5.18×10^3		
x_t [MPa]	1500	σ [MPa]	73
y_t [MPa]	50		

For isotropic materials, the data are introduced by the user, except the shear modulus and the bulk modulus, which are computed from the following expressions, respectively [41]:

$$G = \frac{E}{2(1+v)} \quad (3.2)$$

$$B = \frac{E}{3(1-2v)} \quad (3.3)$$

where E is the elastic modulus and v is the poisson ratio.

3.2.3.2 Static Analysis

A static structural analysis determines the displacements, stresses, strains, and forces in structures. Firstly, the displacements are calculated through the following expression:

$$KU = F \quad (3.4)$$

where *K* is the stiffness matrix of the structure, *U* is the displacement vector and *F* is the external force vector applied to the structure. After displacement’s calculation, the strain and the stress of the structure can be determined.

3.2.3.2.1 Stress and strain formulas for an isotropic material

The following expressions are relative to the strain (ε):

x-direction $\varepsilon_x = \frac{1}{E}\left[\sigma_x - v\left(\sigma_y + \sigma_z\right)\right]$

y-direction $\varepsilon_y = \frac{1}{E}\left[\sigma_y - v\left(\sigma_x + \sigma_z\right)\right]$ (3.5)

z-direction $\varepsilon_z = \frac{1}{E}\left[\sigma_z - v\left(\sigma_x + \sigma_y\right)\right]$

where *E* is Young's modulus and *v* is the Poisson's ratio of the material.

The stress is computed by Hooke's law, as it is represented below:

$$\sigma = C\varepsilon \quad (3.6)$$

In the case of a 3D element and for isotropic materials, C_m is the constitutive matrix given by:

$$[C] = \frac{E}{(1+v)(1-2v)}\begin{bmatrix} 1-v & v & v & 0 & 0 & 0 \\ & 1-v & v & 0 & 0 & 0 \\ & & 1-v & 0 & 0 & 0 \\ & & & \frac{1-2v}{2} & 0 & 0 \\ & & & & \frac{1-2v}{2} & 0 \\ Symmetry & & & & & \frac{1-2v}{2} \end{bmatrix} \quad (3.7)$$

where *E* is the modulus of Young and *v* is the Poisson's ratio of the material [42].

3.2.3.2.2 Stress and strain formulas for an orthotropic material

Fibre-reinforced composites contain, in general, three orthogonal planes of material property symmetry and are classified as orthotropic materials.

The following equation gives the stress-strain relationship:

$$\begin{bmatrix} \sigma_{11} \\ \sigma_{22} \\ \sigma_{33} \\ \sigma_{23} \\ \sigma_{13} \\ \sigma_{12} \end{bmatrix} = \begin{bmatrix} C_{11} & C_{12} & C_{13} & 0 & 0 & 0 \\ & C_{22} & C_{23} & 0 & 0 & 0 \\ & & C_{33} & 0 & 0 & 0 \\ & & & C_{44} & 0 & 0 \\ & & & & C_{55} & 0 \\ Symmetry & & & & & C_{66} \end{bmatrix}\begin{bmatrix} \varepsilon_{11} \\ \varepsilon_{22} \\ \varepsilon_{33} \\ \varepsilon_{23} \\ \varepsilon_{13} \\ \varepsilon_{12} \end{bmatrix} \quad (3.8)$$

These equations can be inverted, introducing elastic constants *E*, *v* and *G*:

$$\begin{bmatrix} \varepsilon_{11} \\ \varepsilon_{22} \\ \varepsilon_{33} \\ \varepsilon_{23} \\ \varepsilon_{31} \\ \varepsilon_{12} \end{bmatrix} = \begin{bmatrix} \frac{1}{E_1} & -\frac{v_{21}}{E_2} & -\frac{v_{31}}{E_3} & 0 & 0 & 0 \\ -\frac{v_{12}}{E_1} & \frac{1}{E_2} & -\frac{v_{32}}{E_3} & 0 & 0 & 0 \\ -\frac{v_{13}}{E_1} & -\frac{v_{23}}{E_2} & \frac{1}{E_3} & 0 & 0 & 0 \\ 0 & 0 & 0 & \frac{1}{2G_{23}} & 0 & 0 \\ 0 & 0 & 0 & 0 & \frac{1}{2G_{13}} & 0 \\ 0 & 0 & 0 & 0 & 0 & \frac{1}{2G_{12}} \end{bmatrix} \begin{bmatrix} \sigma_{11} \\ \sigma_{22} \\ \sigma_{33} \\ \sigma_{23} \\ \sigma_{31} \\ \sigma_{12} \end{bmatrix} \quad (3.9)$$

where E_i is Young's modulus of the material in direction $i=1,2,3$; v_{ij} is the Poisson's ration representing the ratio of a transverse strain to the applied strain, for example, $v_{12}=-\varepsilon_2/\varepsilon_1$, for uniaxial tension in the direction 1 [43].

3.2.3.2.3 Setup

In this section, the procedures are discussed with respect to structural analyses, in a succinct approach, while in Chapter 4 these procedures are applied to each study case, with the results presented and discussion of its.

First, the material should be applied to the structure, which was defined in the last section. Then, a mesh with tetrahedron elements is created. The quality of the mesh is assessed by a mesh metric parameter which provides a value between 0 and 1 based on the geometry of the elements. In this scale, a value closer to 0 indicates lower element quality and a value closer to 1 indicates better element quality. This mesh metric used is "element quality" and it is based on the following expression:

$$Quality = C\left[volume/\sqrt{[[(edge\ length^2]^3]}\right] \quad (3.10)$$

The following table lists the value of C for each type of element.

Table 3.4 – Values of C for each type of element.

Element	C
Triangle	6.92820323
Quadrangle	4.0
Tetrahedron	124.70765802
Hexagon	41.56921938
Wedge	62.35382905
Pyramid	96

The criteria of quality mesh control is defined as 75% of the elements obtain a quality above of 75% and to prove the accuracy of the results is presented the percentage of stress error, in Chapter 4.

After meshing, BCs needed to be applied. For all the analysis, the BCs are the same, which are fixed support, on the faces where spars are intended. The fixed support has the objective of restricting the six degrees of freedom, which are translations and rotations in x, y, and z-axis. Pressure distribution is also applied around the wing surface. This last parameter comes from ANSYS Fluent.

As TO is done after structural analysis, it is not possible to considerer, in this dissertation, the large deflection, since ANSYS TO does not support a solution selection that has deformation turned on. Therefore, small deformation theory is used, i.e. displacements of the material particles are assumed to be much smaller than any relevant dimension of the body, so at each point of space can be assumed to be unchanged by the deformation.

The results of the equivalent stress, total deformation, and strain energy are presented in Chapter 4.

3.2.4 Topological Optimization

When meshing is done in Mechanical and loads are applied and evaluated, the topological optimization can be initiated. All steps in the process necessary to obtain the required results are explained below: analysis settings, optimization region, objective and response constraints.

3.2.4.1 Analysis Settings

In analysis settings, it is possible to define some input settings to the solver. The default maximum number of iterations is 500 but, according to the current problem's objective, this value was set to 2000. The solver will iterate until it converges or until it reaches the maximum number of iterations.

The minimum normalized density is set to 0.001 which the program fully complies with, because for numerical reasons the density of an element cannot be equal to zero.

The convergence accuracy by default is set to 0.1%, but as the objective of this problem is to minimize the mass this value must be 0.05% or lower. The value chosen was 0.04%. The topological optimization solver will approach a stationary point where all constraints will be satisfied within a tolerance of 0.04% of the defined bound.

As explained in section 2.4.3, the penalty factor recommended is $p=3$ to ensure a good convergence and therefore that was the value used.

3.2.4.2 Optimization Region

The geometry to be optimized must be divided into design and exclusion region. The design region is the region that will be optimized, and the exclusion region is a fixed geometry and cannot be optimized by the solver.

In this work, the exclusion region is the wing surface, so the structure maintains the aerodynamic shape, and the spars, and the design region is the wing interior.

3.2.4.3 Response Constraints

The stress constraints are used to prevent the stresses at any point in the domain to exceed a stress level greater than half the yield strength of the material. The response constraint will be von-Mises yield criteria, with a maximum value of 36.5 MPa, which states that yielding occurs when the von Mises stress σ_{vm} equals the yield stress limit σ_{lim}. This yielding constraint is necessary to enforce the assumption of linear elasticity. The von Mises is calculated for each element by the following equation [44]:

$$\sigma_{vm\_i} = \frac{1}{\sqrt{2}}\sqrt{(\sigma_{i1}-\sigma_{i2})^2+(\sigma_{i2}-\sigma_{i3})^2+(\sigma_{i3}-\sigma_{i1})^2+6(\sigma_{i4}^2+\sigma_{i5}^2+\sigma_{i6}^2)} \quad (3.11)$$

where σ_{i1}-σ_{i6} are the stress components for element i.

During the aircraft mission, the performance could not be affected, and so it is necessary to add to this problem the maximum deformation criterion. This constraint is applied on the z-axis, with a correspondent value of 0.1m, which was chosen as being 10% of the wingspan.

3.2.4.4 Objective

Weight reduction of structures is paramount in several industries due to its numerous benefits, such as lower consumption, performance gain and a reduction of material cost. The most common objective in topology optimization is to minimize compliance, which is the same as maximizing the stiffness. Although, in the present case studies the objective of TO problem is the mass minimization. However, weight reduction is constrained by several mechanical failure modes.

SIMP method is described above, assuming constant material density, such that minimizing the mass corresponds to minimizing volume, furthermore, the domain volume is introduced such that the objective function is normalized.

$$Find: X = [\rho_1, \rho_2, \dots, \rho_N]^T$$

$$\text{Min: } m(X)$$

$$s.t. \begin{cases} KU = F \\ kV_{ad} = L_{al} \\ \dfrac{\sigma_{vm_i}}{\sigma_{lim}} \leq 1 \\ \displaystyle\sum_{i=1}^{N} \rho_i \bar{v}_i \leq hV_0 \\ 0 < \rho_{min} \leq \rho_i \leq 1 \end{cases} \qquad (3.12)$$

where X is the design variable vector, ρi design variable of element material density, *m* is the element mass, *N* is the total number of discrete elements, V_0 is the initial volume of the design domain, *h* desired volume ratio, $\tilde{\rho}_i$ is the filtered density, i.e. density now represents the structure, $\bar{v}_i$ is the element volume after optimization, K is the global stiffness matrix, U the global displacement vector, *F* the external force vector, Lal the adjoint load vector, V_{ad} the adjoint displacement vector, ρ_{min} the minimum limit of element relative density and *N* the total number of discrete elements [34, 45]. The element is represented by *i*.

where $\widetilde{\rho_\iota}$ is the filtered density, which is found by a weighted average equation:

$$\widetilde{\rho_\iota} = \frac{\sum_{j=1}^{n_i} w_j \rho_j}{\sum_{j=1}^{n_i} \rho_j} \qquad (3.13)$$

where w_j is the weight function, represented as:

$$w_j = r_{filter} - \|x_j - x_i\| \; if \; \|x_j - x_i\| \leq r_{filter} \qquad (3.14)$$

where r_{filter} is a predetermined mesh filter radius that determines the size of the sphere of influence, as exemplified in Figure 3.7. The weight function decays linearly with distance between element *i* and *j* determined by their respective coordinates x_i and x_j [44].

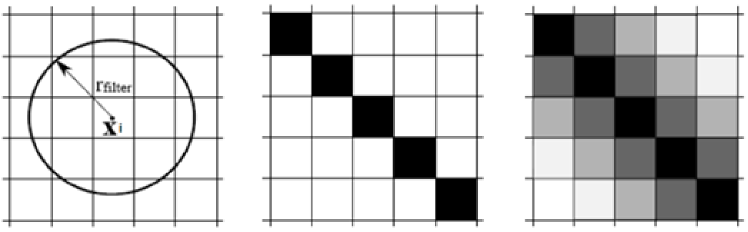

(a) Filter radius and coordinates of element i (b) Design variables (c) Filtered Density

Figure 3.7 – Representation of the effect of the density filter on an arbitrary design variable distribution [44].

The objective function is approximated by a uniformly convex function, while equality constraints, by linear functions and inequality constraints by convex functions as well. So, the optimization problem is replaced by a separable, convex, and nonlinear sub-problem which is easier to solve.

The sensitivities of the material volume $\sum_{i=1}^{N} \rho_i \bar{v}_i$ with respect to the element densities ρ_i are expressed as [34]:

$$\frac{\partial}{\partial \rho_i} \sum_{i=1}^{N} \rho_i \bar{v}_i = \bar{v}_i \quad (3.15)$$

To ensure the convergence of the solution, one may introduce a filtering function that limits the vague minimum width of a member (Sigmund and Petersson 1998). The only drawback of the continuation method is that the number of iterations required to obtain the optimal design may be several hundred [46]. For example, it is widely used 3x3 parametric low pass filter, whose impulse response matrix is defined as [47]:

$$H = \left(\frac{1}{b+2}\right)^2 \begin{bmatrix} 1 & b & 1 \\ b & b^2 & b \\ 1 & b & 1 \end{bmatrix} \quad (3.16)$$

where b corresponds to filter factor, and $b \in [1,\infty[$.

Figure 3.8 presented the importance of *b* factor in optimization, clarifying with the same structure to different b approaches.

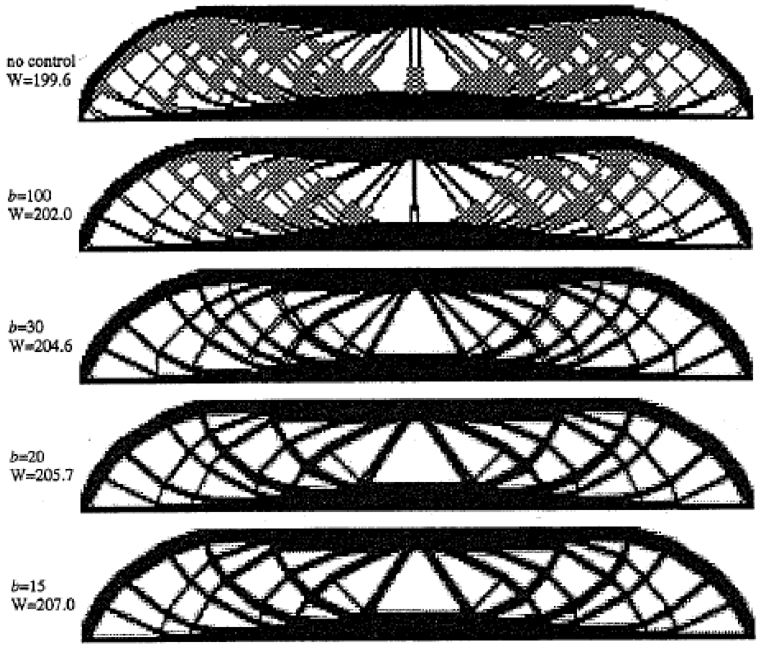

Figure 3.8 – Influence of filter factor b on the optimal layout. The ground structure consists of 120x40=4800 4-node elements and the volume is restricted to 50% of the design domain [47].

Chapter 4

In this chapter different geometries are investigated. First, the study cases used in this work are described. Afterward, a structural analysis is effectuated, and the results are evaluated, in order to proceed to TO. Then, the results from TO are analysed and the study case with lower mass is chosen, which is the main objective of the work. After that, the result obtained in ANSYS TO is transported to CATIA V5 to do a geometry smoothed, leading to a wing final design. Finally, a new structural analysis is realized to investigate the stiffness and strength criterions imposed.

Study Cases

An optimization of a wing was based on the aircraft's data of Air Cargo Challenge 2011, as exemplified in Table 4.1, is presented in this chapter. Figure 4.1 illustrates the aerofoil and in Appendix B there are the aerofoil coordinates. The design must work under certain requirements, bearing all the loads and should be lightweight.

Four geometries were studied in this work. The wing composition was simplified since the focus of the study is removing material from the interior of it. So, no dihedral and sweep were considerate. The proposal wing is rectangular and since the spars are responsible to support bending loads, the geometries have also elements presenting these structural components.

Table 4.1 – Aircraft's data on Air Cargo Challenge 2017.

Data	Value
Maximum weight (take off) [N]	150
Span [m]	2
Chord [m]	0.25
Load factor (maximum)	3

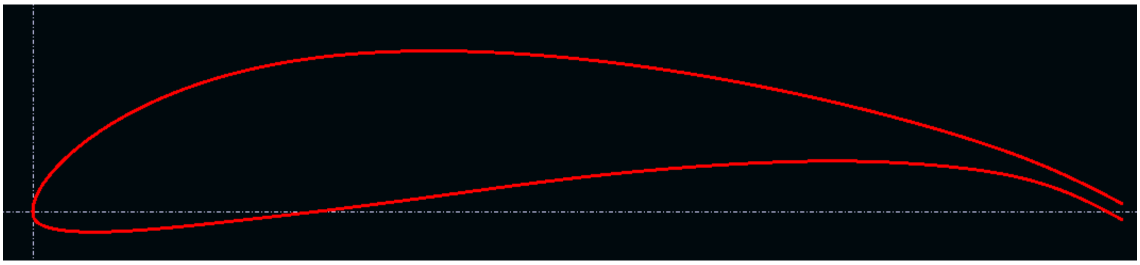

Figure 4.1 – Image of the aerofoil obtained in XFLR5.

The pressure distribution obtained in ANSYS Fluent, as explained in subsection 3.2.2, is used in all of the following case studies.

4.1 Geometry

The focus of this work is the main wing body structure. The analysis considers only the structural support, provided by spars and the wing skin. As follows, all the geometries are described below to a better understanding. Ideally, axisymmetric structures should be made as a continuum structure, free from any junctions or assembly, for the topology optimization.

4.1.1 First Case

The geometry is composed of a rectangular wing with two perforations, that are destined to the spars position, as exemplified in Figure 4.2. The perforation intended to spar, at 25% of the chord, has a diameter of 25mm and the other, at 75% of the chord, has a diameter of 10mm. The material used is PLA.

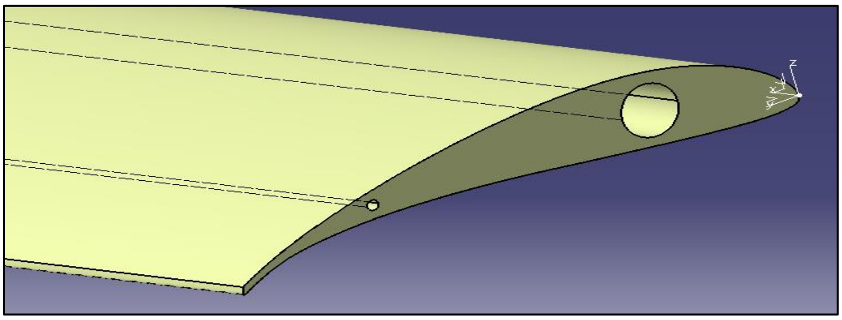

Figure 4.2 – Illustration of the wing root.

4.1.2 Second Case

The geometry is similar to the first one, where PLA is also used. However, the secondary spar is also at the leading edge, as the primary spar, at 10% of the chord. Figure 4.3 illustrates the second case.

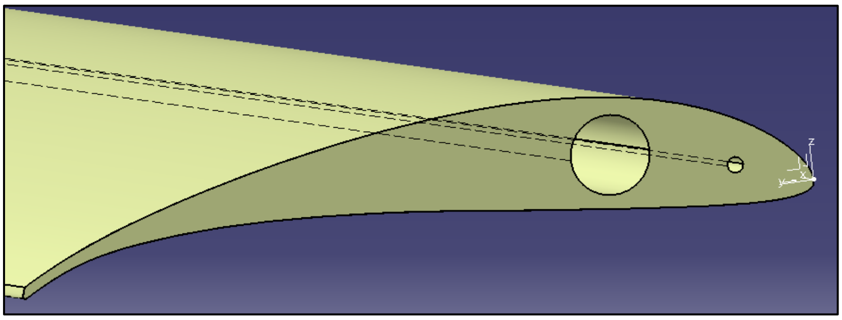

Figure 4.3 – Illustration of the wing root.

4.1.3 Third Case

The geometry, in PLA, is composed of a rectangular wing without spars, at root, it has an element with a diameter of 25mm, at 25% of the chord, and with a thickness of 1mm. This element is to represent the connection between the wing and the fuselage, and with the objective of restricting the existing six degrees of freedom. For better comprehension, Figure 4.4 illustrates the third case.

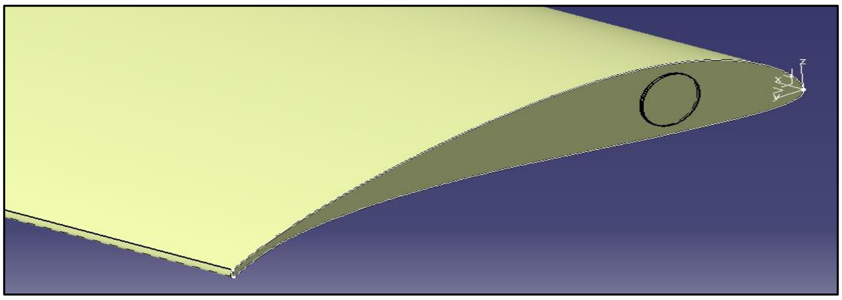

Figure 4.4 – Illustration of the wing root.

4.2 Mechanical

4.2.1 Mesh Element Quality

In Figure 4.5 and in Figure 4.6, the mesh and element quality are presented, respectively, according to the criterion explained in Chapter 3 (3.2.3). Table 4.2 describes the percentage of elements with quality above 75%.

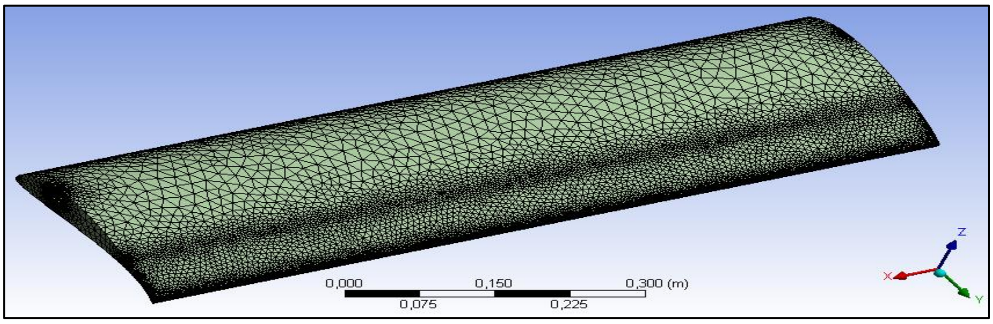

Figure 4.5 – Illustration of mesh, for the first wing study.

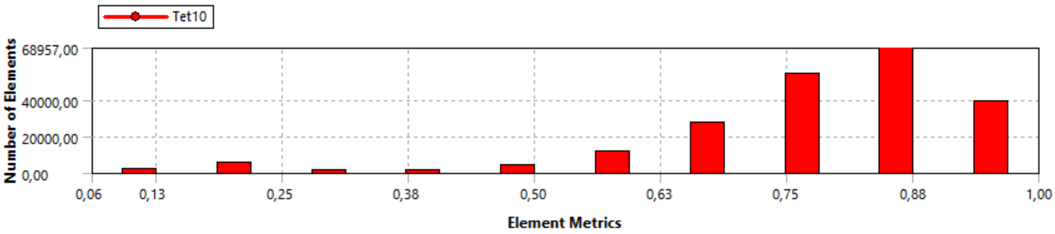

Figure 4.6 – Representation of the element quality, for the first case.

As explained in subsection 3.2.2.1, the type of element in ANSYS is automatically generated, according to the chosen method, which in this work is "Path Conforming Method", where tetrahedrons are the method chosen. The software creates a geometry divided into 10-noded tetrahedron elements, as characterized in Figure 4.7.

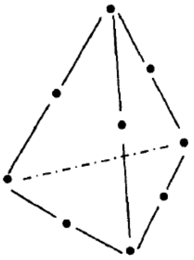

Figure 4.7 – 10-noded tetrahedron element [48].

Table 4.2 – Results from the mesh analysis used on different geometries.

Study Cases	Type of Element	Number of Elements	Percentage of elements with quality above 75%
1	Tet10	216657	75.1%
2	Tet10	230861	75%
3	Tet10	397679	83.4%

After defining the mesh, BCs can be applied, as explained in section 3.2.3.

After the results of elements percentage with quality above 75%, it must be verified that there is convergence mesh, i.e. a balance between the accuracy of results and the computational analysis. The point of mesh convergence is the point where the mesh refinement no longer changes the results obtained. To interpret where mesh refinement is required, ANSYS percentage stress error helps. This analyse is defined as the stress error energy divided by the total strain energy. It is possible to define an expression to plot the percentage stress error, establishing strain energy as ENERGY POTENTIAL and the absolute stress error energy as SERR, resulting in the following formula:

$$(\mathrm{SERR}/\mathrm{ENERGYPOTENTIAL})\times 100 \quad (4.1)$$

For the region of interest, the aim is to have a percentage of stress error below 5% or 10%.

4.2.2 Results

The results are presented below: Figures 4.8 the distribution of equivalent stress is illustrated; Figures 4.9 represent the total deformation over the wing; and Figures 4.10 show the percentage of stress error, which is a rigorous way to control the accuracy of the results. In equivalent stress and deformation images, there are minimum and maximum indicators. Table 4.3 provides the data for the three structural study parameters and the corresponding mass.

Table 4.3 – Results from Mechanical analysis.

Study Cases	**Equivalent Stress [Pa]**		**Total Deformation [m]**		**Strain Energy [J]**		**Mass [kg]**
	Maximum	Minimum	Maximum	Minimum	Maximum	Minimum	
1	92418	3.8424	7.2112×10^{-6}	0	7.1124×10^{-9}	3.4334×10^{-19}	6.1055
2	52468	6.4659	1.7548×10^{-5}	0	1.3604×10^{-7}	1.2648×10^{-18}	6.1055
3	1.4355×10^{8}	136.77	18.605×10^{-3}	0	7.6812×10^{-4}	4.1474×10^{-16}	6.7391

4.2.2.1 Equivalent Stress

Relatively to the first case, the maximum equivalent stress of the structure is 92418Pa, presenting this value at the trailing edge of the wing root. It has also a brittleness of 34659Pa on the surface around the secondary spar, while the rest of the structure has a value of 3.84Pa. The second case shows a maximum value at the wing tip, of 52468Pa. As the secondary spar is at the leading edge, the structure presents a minimum value, 6.5Pa there and at the trailing edge, while between reaches at 34981Pa. The third case is almost uniform, yielding a minimum value for the entire wing of 136.8Pa, while the maximum, of 1.44×10^{8}, is in the structure that represents the connection point wing-fuselage. Stress levels were maintained in wing structure at acceptable levels of specified limit, which is 36.5×10^{6}, according to PLA ultimate tensile strength.

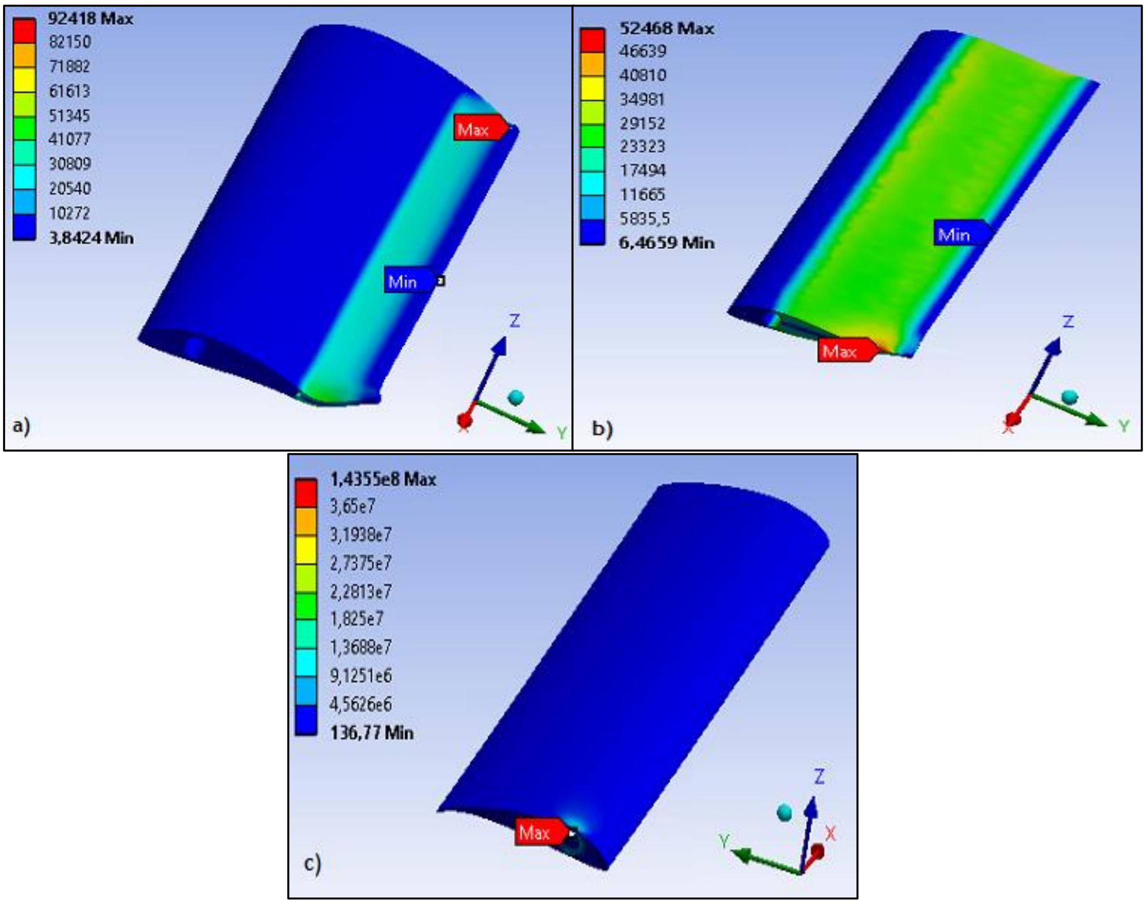

Figure 4.8 – Distribution of equivalent (von-Mises) stress over the wing, in Pa, where: a) first case, b) second case and c) third case.

4.2.2.2 Total Deformation

For the first and second cases the maximum value is at the wing tip, and the increasing distribution goes from the leading edge to the trailing edge, where the minimum is at the leading edge. For the third, the maximum value is also at the wing tip, but the increasing distribution goes from the wing root to the wing tip.

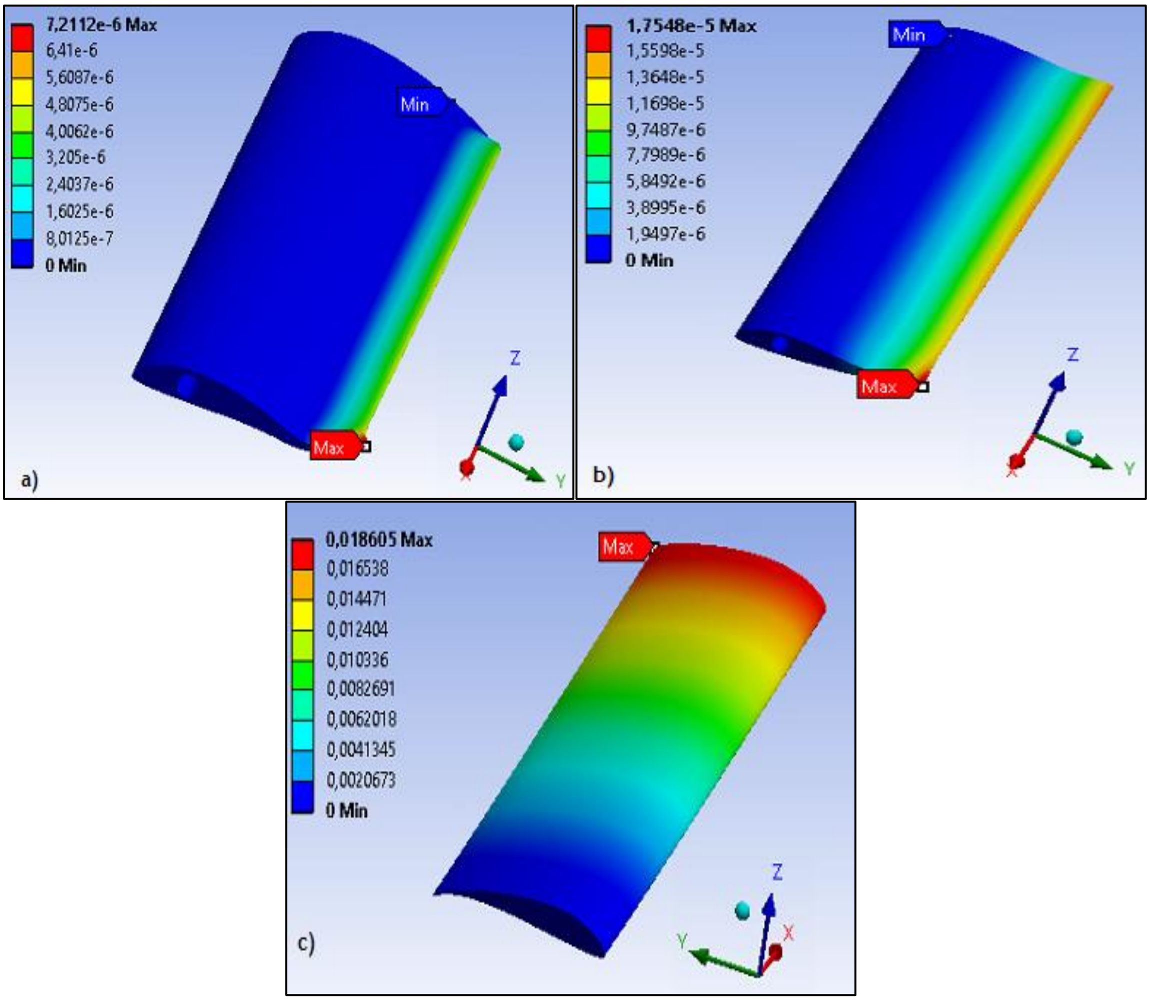

Figure 4.9 – Distribution of deformation over the wing, in m, where: a) first case, b) second case and c) third case.

4.2.2.3 Percentage of Stress Error

For all the cases the percentage of stress error proves that results are accurate, demonstrating good mesh quality.

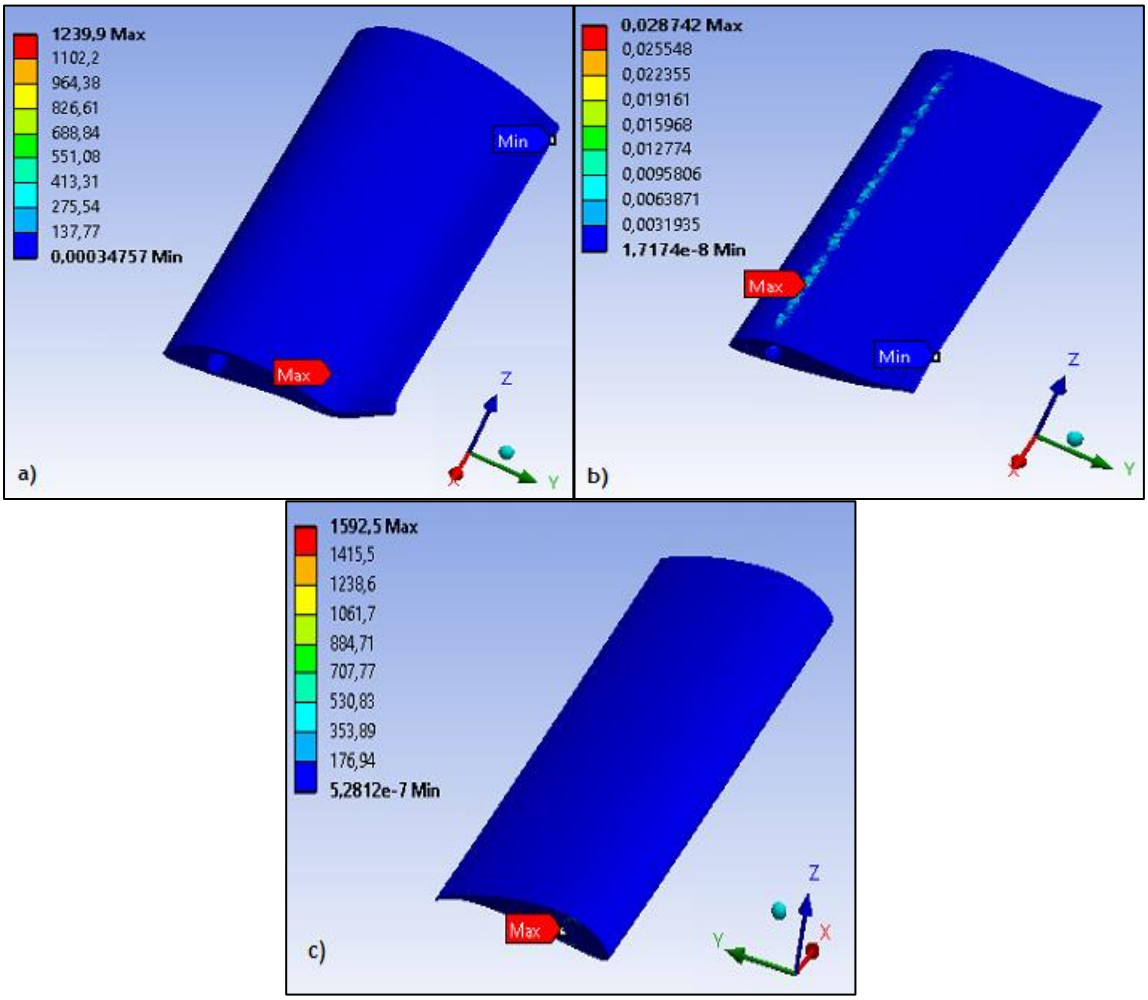

Figure 4.10 – Percentage of stress error, where: a) first case, b) second case and c) third case.

4.3 Topology Optimization

After the results from Mechanical analysis, TO can be accomplished. The results from the TO are evidenced, according to the parameters described in subsection 3.2.4.

4.3.1 Optimization Region

Figures 4.11, 4.12 and 4.13 shows where the design region and the exclusion region are located. The design region is illustrated in blue and the exclusion is in red and the wing root is represented at right of the images and the tip is at left.

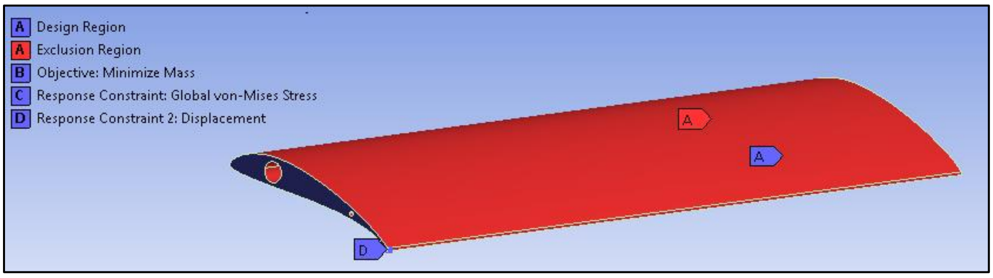

Figure 4.11 – Representation of exclusion and design regions, for the first case.

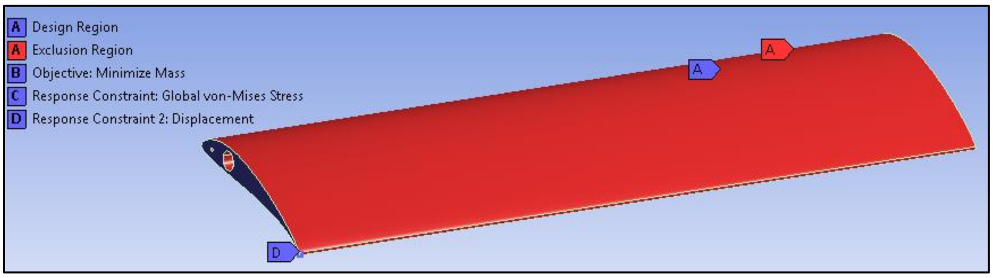

Figure 4.12 – Representation of exclusion and design regions, for the second case.

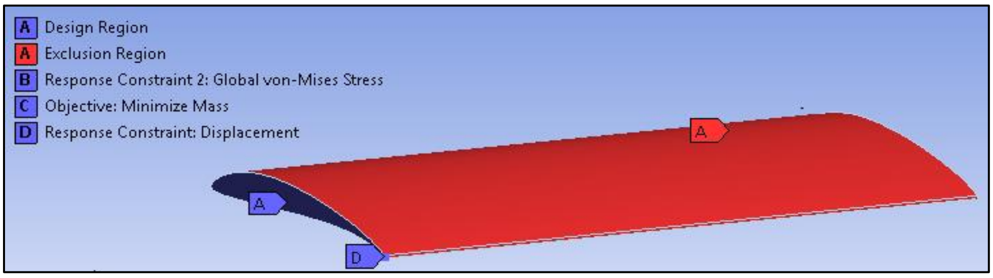

Figure 4.13 – Representation of exclusion and design regions, for the third case.

4.3.2 Results

After setting the analysis parameters, the objective and optimization region defined, the results can be obtained. In Table 4.4 results from the TO are exemplified and Figures 4.14 and 4.15 illustrate where the removed and retained material are, respectively, for the first case. Figures 4.16 and 4.17 exemplify in the second case. The third case corresponds to Figures 4.18 and 4.19. In Appendix C is presented for the four cases images illustrating graphics of the objective convergence, variation of global stress response and variation of displacement response.

Table 4.4 – Results of the Topology Optimization, to the different study cases.

Study Cases	Original Volume [m^3]	Final Volume [m^3]	Final Mass [kg]	Iteration Number
1	4.9147×10^{-3}	3.9482×10^{-3}	4.8957	6
2	4.9147×10^{-3}	4.1071×10^{-3}	5.0928	6
3	5.4257×10^{-3}	1.9222×10^{-3}	2.3835	231

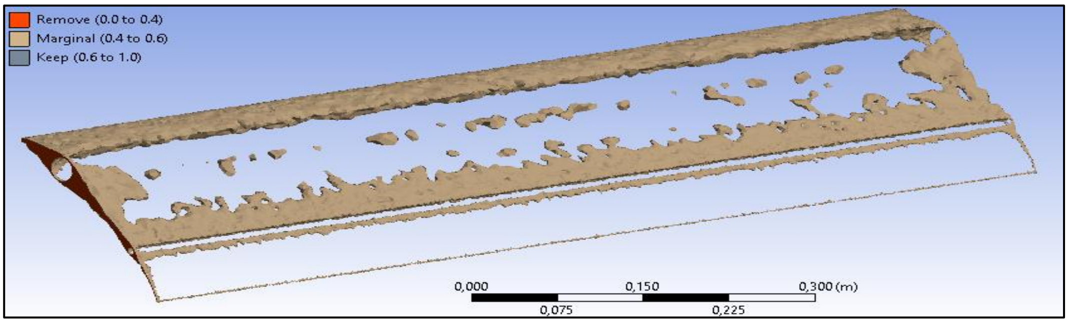

Figure 4.14 – Representation of the removed material, of the first case.

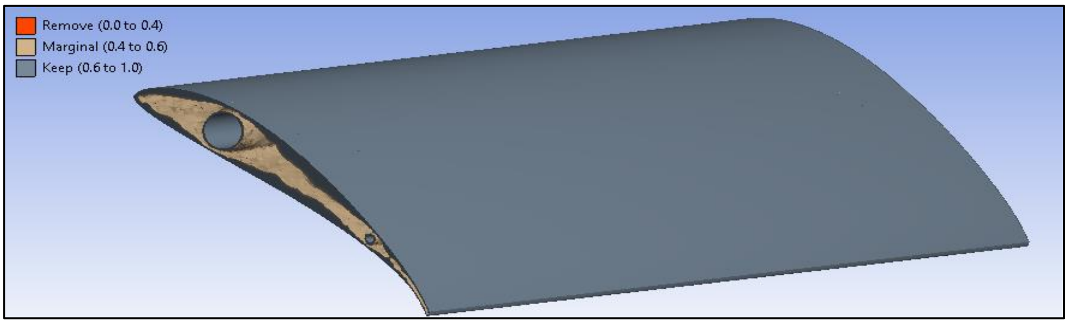

Figure 4.15 – Representation of the retained region, of the first case.

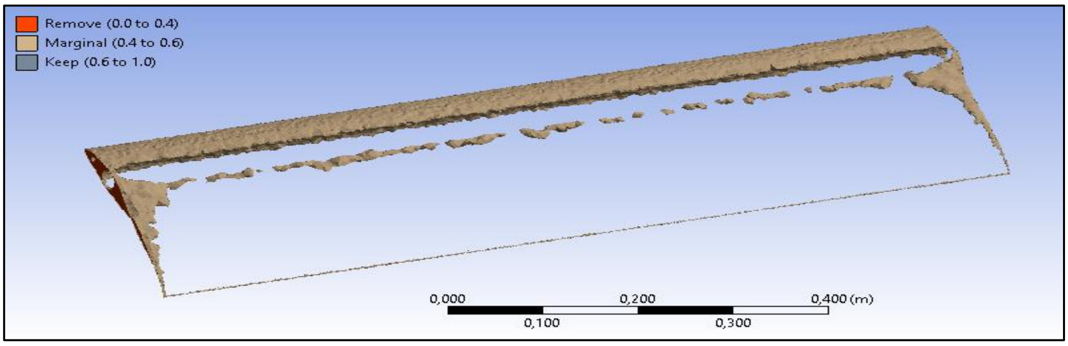

Figure 4.16 – Representation of the removed material, of the second case.

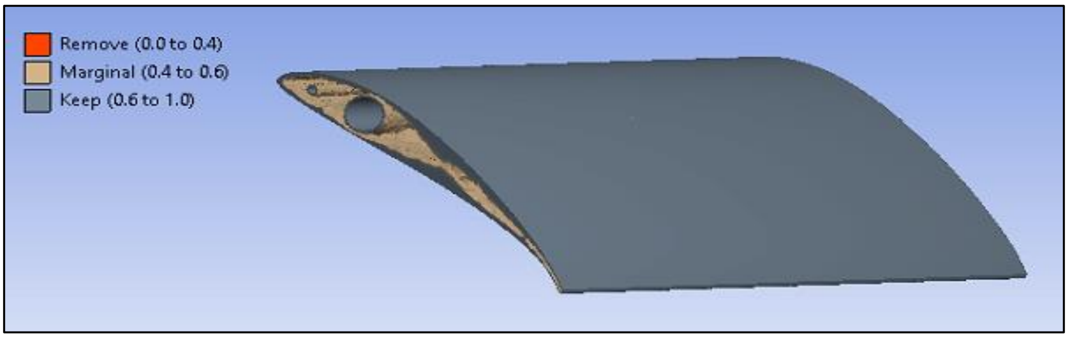

Figure 4.17 – Representation of the retained region, where the tip of the wing is detached, of the second case.

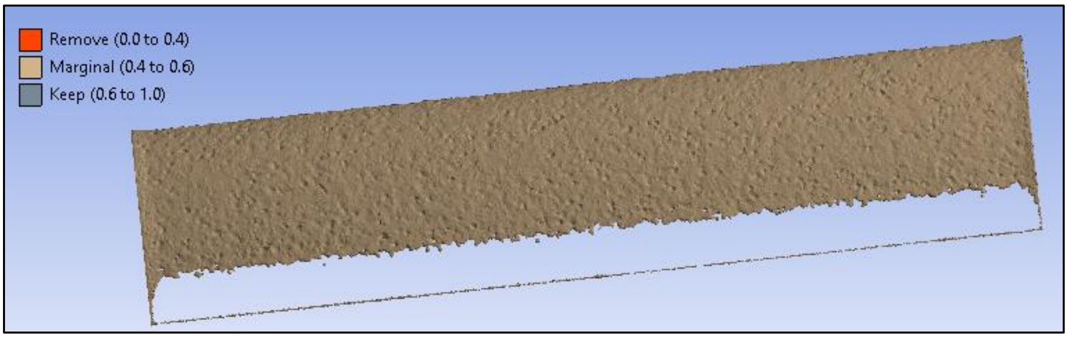

Figure 4.18 – Representation of the removed material, of the third case.

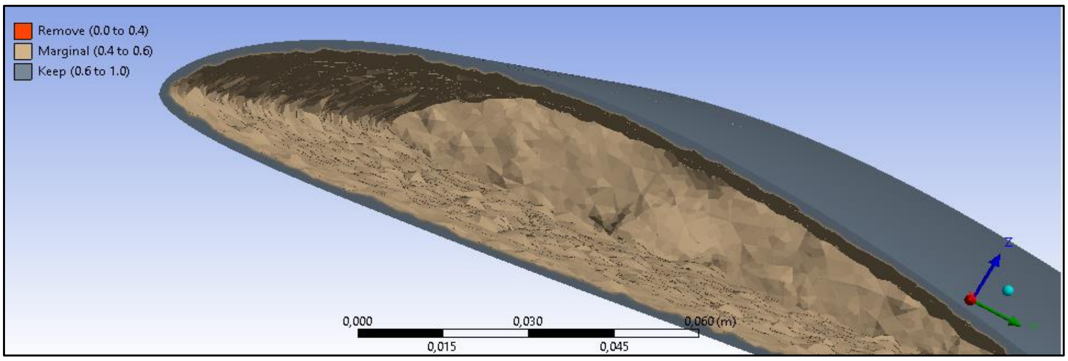

Figure 4.19 – Representation of the retained material, of the third case. The image focus on wing' tip to the interior.

Concerning to analyses, ANSYS TO only support 3D geometries with 20, 10 or 8 nodes. In present work geometries were defined by 10 nodes, i.e. it has three degrees of freedom at each node: translations in the nodal x, y and z directions. The elements have plasticity, stress stiffening, and large strain capabilities. Nevertheless, TO does not support large-deflections effects in static structural analysis, as referred previously, nonlinear contacts, axisymmetric model when is defined a global von-Mises stress constraint and local von-Mises stress constraint, and initial type boundary conditions, i.e. acceleration, standard earth gravity, rotational velocity, and rotational acceleration.

Having said that, the results are analysed afterward. In the first and second cases, the final mass is similar, demonstrating that the position of the secondary spar has no influence in the optimization. Although the objective function in the sixth iteration has converged, the convergence values for global stress and for displacement were distant from the established criterions. These results can be observed in Appendix C, in C.1 – First Case and C.2 – Second Case.

In the third case, with the minimum final mass compared with the other cases, the convergence value of global stress response was coincident with the defined criterion, while the convergence value of displacement was too distant from the criterion, as illustrated in Appendix C, in C.3 – Third Case. According to the figures of the appendix, it is possible to observe that the convergence value of global stress was from the 12th iteration, approximately, coincident with the value of global stress criterion. This correspondence is justified due to the maximum structural result on the equivalent (von-Mises) stress is higher than the yield stress limit, and this could be a possible cause for the optimization model not remove more material from the structure. However, the local where the maximum was detected was designated previously as non-space in TO. So even achieving better results, when compared to others, the combined objective convergence should only stop when the displacement response criterion was coincident with displacement response convergence.

In Appendix C, Figures C.1, C.3, and C.5 show the objective convergence criterion, which in all cases is the mass minimization. The objective convergence criterion considers the design variables, strength, and stiffness, according to equation 3.12. As the objective is to minimize the mass, in Figure C.1 and C.3, when ANSYS detects an increasing of objective function value stops the iterations and assume convergence. In the third case, it was different, because the objective function value in 230th decreases, reaching a value well below the combined objective convergence criterion, and as in 231th the value become the same the program assumes the convergence.

During the iterations neither the dynamics of the system nor the topology is physically correct, due to the stiffness and mass of the geometry change significantly, even so, it converges to a correct result, both for topology and dynamical behaviour, assuming that the thickness of the elements of the final result is either one or zero.

4.4 Post-processing and design verification

The results from Topology Optimization can be transferred to the Design Validation System, which is very accurate for post-processing possibilities. At SpaceClaim, two geometries are transferred, the geometry before optimization and the other after TO, for providing an easier post-process.

As the results from the first and second, in terms of final mass, these geometries are excluded from the post-processing. Although the third geometry has been a final mass too high from the expected, due to the weight of the UAV being 5kg, post-processing of the geometry is done, in CATIA, and then a design verification.

The design verification is a test that ensures that the final product fulfils the specified requirements, under specified operating conditions. In this case, the geometry will be exported again to the ANSYS Mechanical and will be submitted to a distribution of pressure and loads, to see if it verifies the strength and stiffness criterions.

4.4.1 Final design

A model was created, based on the result from topology optimization for the third case, with a thick shell of 2mm, as showed in Figure 4.20 and 4.21. From 75% of the chord to the trailing edge, it is all covered by PLA material.

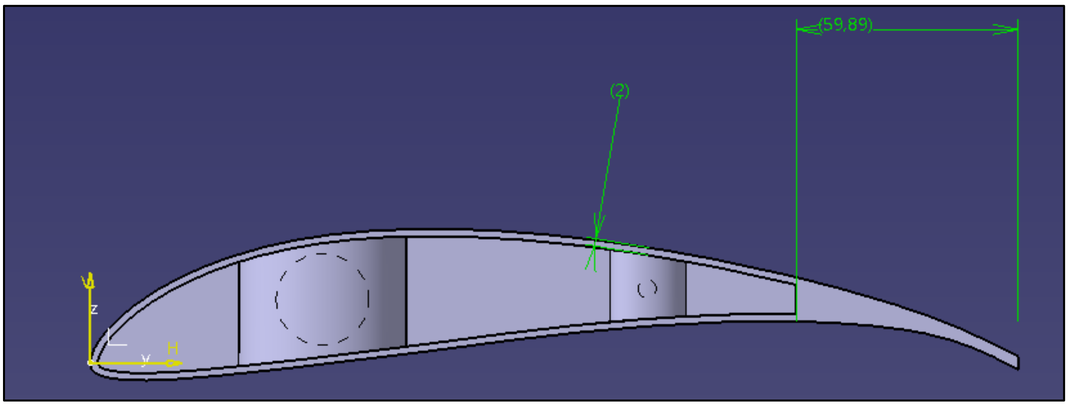

Figure 4.20 – Representation of the final geometry, as viewed from the side, in CATIA.

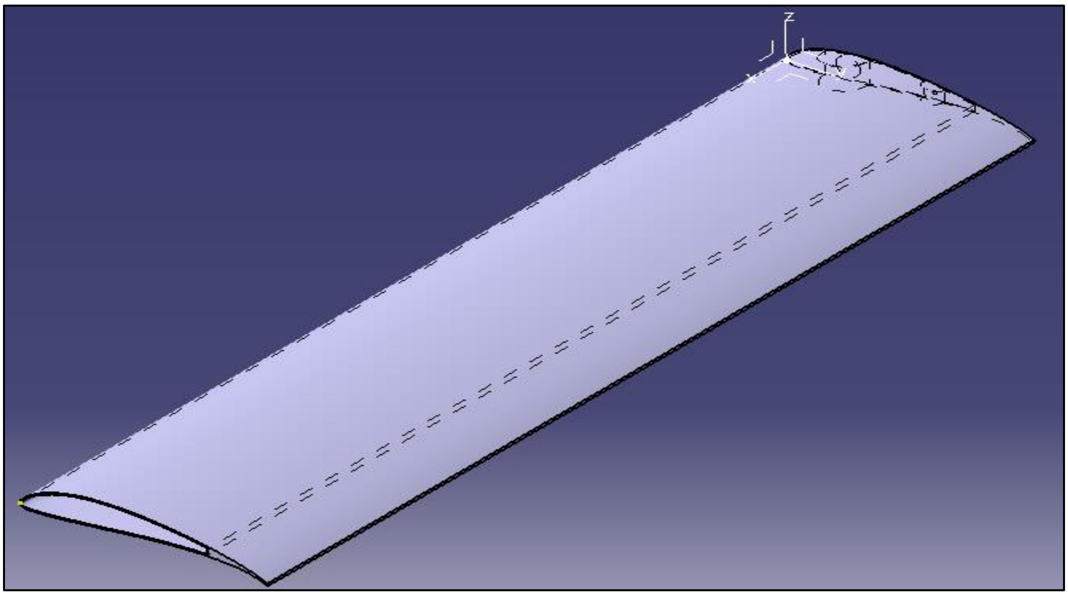

Figure 4.21 – Representation of the optimized geometry, from the top, in CATIA.

High stress can be decentralized by adding structural elements, as it was done in the root wing, between the wing-fuselage connection. Figure 4.22 shows the structural elements and in Appendix D it is possible to a better perception of elements dimensions. Reducing the stress concentration factor under static load will increase the fatigue endurance of the component.

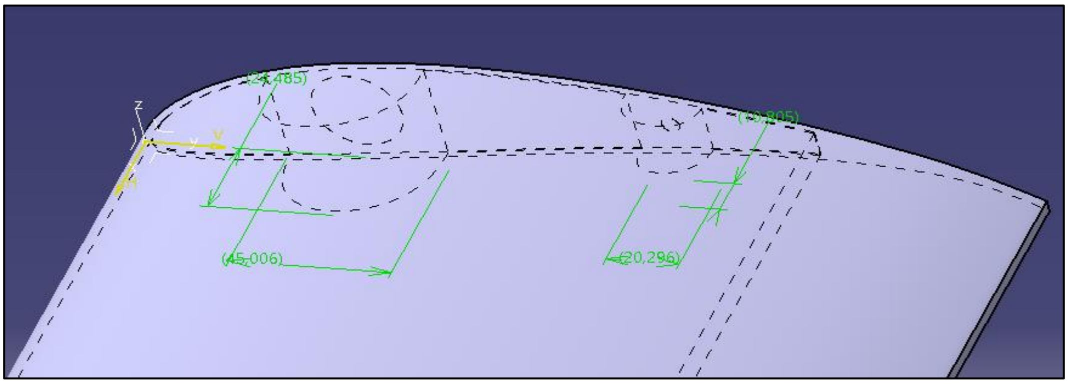

Figure 4.22 – Representation of the support from the connection between wing-fuselage.

4.4.2 Structural Analysis

Table 4.5 has the data of final design, with respect to von-Mises stress and total deformation results. Figures 4.23 and 4.24 complete the analyse.

Table 4.5 – Results of the final design, obtained in ANSYS.

Equivalent Stress [Pa]		Total Deformation [m]		Strain Energy [J]		Mass [kg]
Maximum	Minimum	Maximum	Minimum	Maximum	Minimum	
9.4252×10^{7}	350.88	4.7299×10^{-2}	0	2.2556×10^{-3}	2.4165×10^{-13}	1.5201

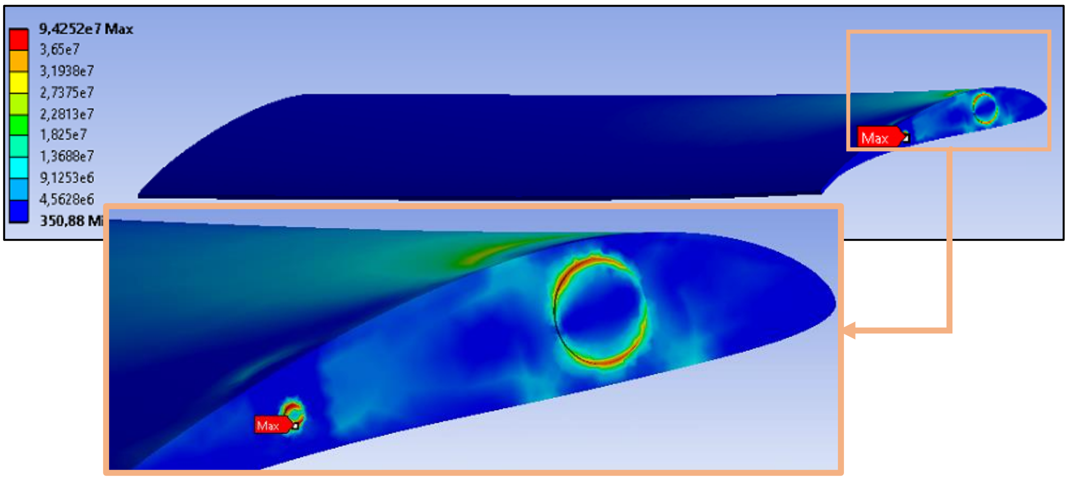

Figure 4.23 - Distribution of equivalent (von-Mises) stress over the wing, in Pa.

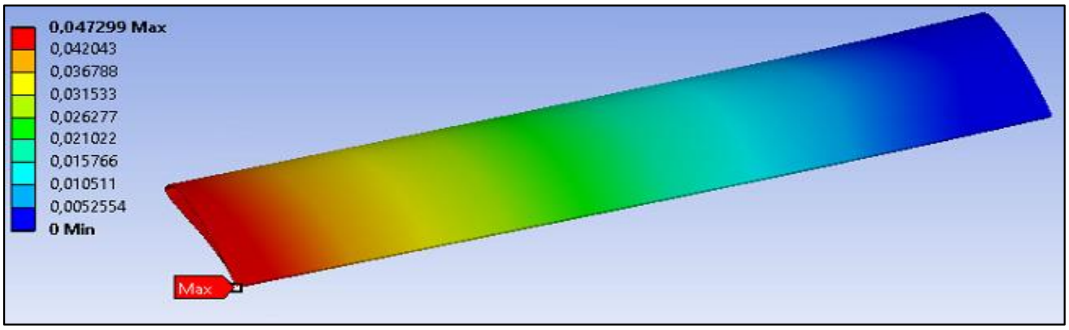

Figure 4.24 – Distribution of deformation over the wing, in m.

The maximum value of equivalent stress is located in the structure where is represented the spar, as occurred in the mechanical analysis of the third case. Although the maximum value of equivalent stress is higher from the expected, 36.5×10^{6}Pa, is only local, with a small volume. Unidirectional carbon fibre reinforced plastic (mentioned in 3.2.3.1) can be applied to this element since bear higher strength compared to PLA. Concerning to deformations, the maximum value is at the wing tip, however, is less than 10% of the wingspan.

Chapter 5

Conclusions and Future Work

5.1 Conclusions

All the proposed tasks were concluded. The most important objective was the TO, and after different analysis, a lighter structure was proposed, which was obtained through the third study case.

Firstly, a CFD analysis was executed. The k-epsilon (ε) was chosen. Then, to determine the performance, structural analyses were performed, where the chosen parameters were: von-Mises equivalent stress, total deformation, and strain energy. After the results obtained from the Mechanical, TO was initiated. The results from the equivalent von-Mises stress showed that the maximum stress created within the body is much smaller, around 0.25% of the limit in the wing structure imposed than the tensile limits of the materials.

As referred initially, the third case was used to obtain the final design, excluding from this process the first and second cases due to their final weight. After TO, a 64% reduction in structural weight was achieved. Following that, a smooth process in CATIA was performed, resulting in a final mass of 1.5 kg. Nevertheless, this design is susceptible for future TO, since the final weight is still heavier than the desired one for the required UAV.

As mentioned in Chapter 2, AM is used specially to create complex geometries, without any obstacle, like tool or moulds barriers as the traditional methods. It was expected that the final geometry provided by ANSYS TO, was a complex one, but the software created a wing with thick skin, without any complex structures inside the wing surface. And for this reason, 3D printing was excluded.

TO achieve stiffness and strength condition, i.e. TO did not create structures that exceeded the imposed criterions. Either, obtain results where the mass value reduces, although it was not enough. Concluding, this method was not appropriate for these geometries since the equivalent stress of the wing structures are below from the imposed limit, 36.5×10^{6}Pa.

5.2 Challenges

With the accomplishment of this works some challenges have arisen. The principal challenge was the computational time, due to be an analysis with 3D geometries. The CFD and TO analysis were fully dependent on the computational time cost, leading to simulations longing for several days.

During topological optimization was created in geometries some discontinuities and irregularities as the method remove material from the reference domain of structures. The phase more challenging was the post-processing, where the geometry obtained was transferred to SpaceClaim, a CAD software integrated into ANSYS. The mesh created previously is also transferred and the hard task is to remove it because the transition to tetrahedron elements to bigger elements creates more discontinuities in geometry, i.e. a face with curvature in some cases can be transformed in a plate, which in this work cannot happen because affects the aerodynamic performance. In some cases, it was possible to maintain the curvature of faces, however, to analyse structurally the optimized geometry it is necessary to create other mesh, many times above the other which succeed in results with smaller accuracy or non-accuracy. So, for this reason, CATIA was the software chosen to do the post-processing.

Another challenge was the design verification. A final geometry was created with thickness variation, this is, the difference in thickness from the root to the wing tip however ANSYS could not do the structural analysis, due to geometry contacts (Rigid body – maximum contact stiffness was too big).

5.3 Future Work

The following topics were noted as future work to continue the study of topology optimization for unmanned aircraft wings:

- A further study will be completed to determine the possibility of using internal components, like load-bearing structures.
- A further investigation with other software using topology optimization, comparing the results with the Matlab code written by Ole Sigmund [49].
- Another investigation could be making the aerodynamic and structural study of a 3D wing. Then, where the parameters are similar the geometry could be turned into a 2D one, with the objective of making a TO, and then with the resulting geometry, replicate it in order to obtain again a 3D structure. In this way, computational time is saved, and complex structures could be obtained.

For all the previous topics AM should be considered.

Bibliography

[1] M. Baumers, P. Dickens, C. Tuck e R. Hague, “The cost of additive manufacturing: machine productivity, economies of scale and technology-push,” *Technological Forecasting and* , vol. 102, pp. 193-201, 2016.

[2] J. V. Silva e R. A. Rezende, “Additive Manufacturing and its future impact in logistics,” em *6th IFAC Conference on Management and Control of Production and Logistics*, Fortaleza, Brazil, 2013.

[3] S. A. Tofail, E. P. Koumoulos, A. Bandyopadhyay, S. Bose, L. O'Donoghue e C. Charitidis, “Additive manufacturing: scientific and technological challenges, market uptake and opportunities,” *ELSEVIER,* 2017.

[4] I. Gibson, D. W. Rosen e B. Stucker, Additive Manufacturing Technologies, Springer, 2010.

[5] N. Gardan e A. Schneider, “Topological optimization of internal patterns and support in additive manufacturing,” *Journal of Manufacturing Systems,* vol. 37, pp. 417-425, 2015.

[6] J. R. C. Dizon, A. H. E. Jr., Q. Chen e R. C. Advincula, “Mechanical characterization of 3D-printed polymers,” *Additive Manufacturing,* vol. 20, pp. 44-67, 2018.

[7] C. Fero, R. Grassi, C. Seclì e P. Maggiore, “Additive Manufacturing Offers New Opportunities in UAV Research,” *Procedia CIRP,* vol. 41, pp. 1004-1010, 2016.

[8] G. Goh, S. Agarwala, G. Goh, V. Dikshit, S. Sing e W. Yeong, “Additive manufacturing in unmanned aerial vehicles (UAVs): Challenges and potential,” *Aerospace Science and Technology,* vol. 63, pp. 140-151, 2017.

[9] G. Gomez-Gras, R. Jerez-Mesa, J. A. Travieso-Rodriguez e J. Lluma-Fuentes, “Fatigue performance of fused filament fabrication PLA specimens,” *Materials and Design,* vol. 140, pp. 278-285, 2018.

[10] A. Silva, *Materiais de Construção Aeroespacial,* Universidade da Beira Interior, 2017.

[11] D. Caputo, P. Aprea, N. Gargiulo e B. Liguori, “The Role of Materials and Products Characterization in the Additive Manufacturing Industry,” em *IEEE 3rd International Forum on Research and Technologies for Society and Industry (RTSI)*, Modena, Italy, 2017.

[12] J. Torres, J. Cotelo, J. Karl e A. P. Gordon, “Mechanical Property Optimization of FDM PLA in Shear with Multiple Objectives,” *The Minerals, Metals & Materials Society,* vol. 67, 2015.

[13] Y. Song, Y.Li, W. Song, K. Yee, K.-Y. Lee e V. Tagarielli, “Measurements of the mechanical response of unidirectional 3D-printed PLA,” *Materials and Design,* vol. 123, pp. 154-164, 2017.

[14] AMRC, “FDM-printed fixed wing UAV,” [Online]. Available: https://www.amrc.co.uk/case-studies/fdm-printed-fixed-wing-uav. [Acedido em 6 Março 2018].

[15] U. o. Southampton, “Flying on printed wings,” *New Scientist,* 2011.

[16] Southampton, “Southampton engineers fly the world's first 'printed' aircraft,” [Online]. Available: https://www.southampton.ac.uk/engineering/news/. [Acedido em 14 Abril 2018].

[17] Aurora Flight Sciences, “World's first jet-powered, 3D-printed UAV debuts at Dubai Airshow,” NEW ATLAS, [Online]. Available: https://newatlas.com/worlds-largest-fastest-3d-printed-uav/40293/. [Acedido em 15 Abril 2018].

[18] 3D LabPrint, “EASYMAX001,” [Online]. Available: https://3dlabprint.com/shop/easymax-001/. [Acedido em 16 Abril 2018].

[19] K. Goodmanson, C. Mazurek, S. McConomy e F. Wheeler, “Rapid Prototype Manufacturing for an Advanced Composite Wing Structure,” University of Manitoba, 2011.

[20] D. Walker, D. Liu e A. Jennings, “Topology Optimization of an Aircraft Wing,” em *56th AIAA/ASCE/AHS/ASC Structures, Structural Dynamics, and Materials Conference*, Kissimmee, Florida, 2015.

[21] L. Xue-ping, Z. Lian-yu e L. Zheng-zhong, “Topological Optimization of Continuum Structure based on ANSYS,” *MATEC Web of Conferences,* vol. 95, 2017.

[22] A. Aremu, I. Ashcroft, R. Hague, R. Wildman e C. Tuck, *Suitability of SIMP and BESO Topology Optimization Algorithms for Additive Manufacture,* Wolfson School of Mechanical and Manufacturing Engineering, UK, 2010.

[23] P. M. C. Carneiro, “Investigação e otimização de nervuras obtidas através de fabrico aditivo,” Tese de Mestrado. Universidade da Beira Interior , Covilhã, 2017.

[24] F. Jensen, “Topology Optimization of Turbine Manifold in the Rocket Engine Demonstrator Prometheus,” Degree Project. Lulea University of Technology, 2018.

[25] C. A. Veloso, D. C. Martins, R. A. Costa e P. Júnior, “Análise estrutural da asa da aeronave A320 a partir do carregamento aerodinâmico,” em *XXXVII IBERIAN LATIN AMERICAN CONGRESS ON COMPUTATIONAL METHODS IN ENGINEERING*, Brasília, Brasil, 2016.

[26] S. K. Tippabhotla, *Introduction to Finite Element Analysis using ANSYS,* Singapore University of Technology and Design.

[27] E. Madenci e I. Guven, The Finite Element Method and Applications in Engineering Using ANSYS, Springer, 2006.

[28] G. Rozvany, “A critical review of established methods of structural topology optimization,” em *Structural and Multidisciplinary Optimization*, Springer-Verlag, 2009, pp. 217-237.

[29] Z. H. Zuo e Y. M. Xie, “Evolutionary topology optimization of continuum structures with a global displacement control,” *Computer-Aided Design*, vol. 56, pp. 58-67, 2014.

[30] K. A. James, G. J. Kennedy e J. R. Martins, “Concurrent aerostructural topology optimization of a wing box,” *Computers and Structures,* vol. 134, pp. 1-17, 2014.

[31] F. Sousa, F. Lau e A. Suleman, “Topology optimization of a wing structure,” 2016. [Online]. Available: https://www.researchgate.net/publication/287070035_Topology_optimization_of_a_wing_structure. [Acedido em 18 Outubro 2018].

[32] G. Rozvany, “Aims, scope, methods, history and unified terminology of computer-aided topology optimization in structural mechanics,” em *Structural and Multidisciplinary Optimization*, Springer, 2001, pp. 90-108.

[33] S.Liu, Q.Li, J.Liu, W.Chen e Y.Zhang, “Realization Method for Transforming Topology Optimization Design to Additive Manufacturing Structures,” *Engineering,* 2018.

[34] T. Xinxing, G. Wenjie, S. Chao e L. Xiaoyong, “Topology optimization of compliant adaptive wing leading edge with composite materials,” *Chinese Journal of Aeronautics,* vol. 27, pp. 1488-1494, 2014.

[35] Y. Nakasone, S. Yoshimoto e T. Stolarski, Engineering Analysis with ANSYS Software, Elsevier, 2006.

[36] “Ozen,” ENGINEERING, Inc, [Online]. Available: https://www.ozeninc.com/ansys-workbench/. [Acedido em 29 Outubro 2018].

[37] ANSYS, Inc., ANSYS FLUENT Theory Guide, 2011.

[38] ANSYS, *Lecture 8 - Mesh Quality. Introduction to ANSYS Meshing,* 2014.

[39] P. V. Gamboa, “Projeto de Aeronaves,” [Online]. Available: http://webx.ubi.pt/~pgamboa/pessoal/10403/apontamentos/capitulo12.pdf. [Acedido em Fevereiro 2019].

[40] L. Zhao, Y. Gong, T. Qin, S. Mehmood e J. Zhang, “Failure prediction of out-of-plane woven composite joints using cohesive element,” *Composite Structures,* nº 106, pp. 407-416, 2013.

[41] S. Imaoka, “Analyzing Viscoelastic Materials,” *ANSYS Advantage,* vol. II, nº 4, pp. 46-47, 2008.

[42] M. C. G. Esteves, “Design Optimization for AM of MECSE CubeSat's Mechanical System,” Tese de Mestrado. Universidade da Beira Interior, Covilhã, 2018.

[43] Kelly, “Anisotropic Elasticity,” em *Solid Mechanics Part I,* pp. 156-166.

[44] J. E. K. Hersboll, “3D Topology Optimization with Fatigue Constraints,” Project. Aalborg University, 2018.

[45] W. Zhang, W. Zhong e X. Guo, “An explicit length scale control approach in SIMP-based topology optimization,” *Computer Methods in Applied Mechanics and Engineering,* vol. 282, pp. 71-86, 2014.

[46] X. Huang e Y. M. Xie, "Evolutionary topology optimization of continuum structures with an additional displacement constraint," em *Structural and Multidisciplinary Optimization*, Springer-Verlag, 2010.

[47] O. Sigmund, *Design of Material Structures Using Topology Optimization,* Technical University of Denmark, December 1994.

[48] G. L. Narasaiah, "Chapter 6 - High Order and Isoparametric Elements," em *Finite Element Analysis*, BS Publications, 2008, p. 168.

[49] M. Bendsoe e O. Sigmund, Topology Optimization. Theory, Methods and Applications, Springer, 2003.

Appendixes

Appendix A

Table A.1 – Results from XFLR5, to a fixed speed of 24 m/s.

A [°]	C_L	C_{Di}	C_D	C_m	V [m/s]	XCP	L [N]
-5	0,508441	0,011601	0,011601	-0,44856	24	0,2233	42,72124658
-4	0,59088	0,015341	0,015341	-0,46953	24	0,2006	49,64810112
-3	0,673035	0,019601	0,019601	-0,49039	24	0,1834	56,55109284
-2	0,754855	0,024373	0,024373	-0,51113	24	0,17	63,42593652
-1	0,836288	0,029649	0,029649	-0,5317	24	0,1593	70,26826291
0	0,917283	0,035418	0,035418	-0,55209	24	0,1505	77,07378679
1	0,997788	0,041667	0,041667	-0,57227	24	0,1431	83,83813891
2	1,077754	0,048385	0,048385	-0,59223	24	0,1369	90,5572021
3	1,157132	0,055554	0,055554	-0,61192	24	0,1315	97,22685917
4	1,235873	0,063159	0,063159	-0,63134	24	0,1269	103,842993
5	1,31393	0,071183	0,071183	-0,65045	24	0,1229	110,4016543
6	1,391257	0,079605	0,079605	-0,66923	24	0,1193	116,8989782
7	1,467809	0,088406	0,088406	-0,68767	24	0,1161	123,3311834
8	1,543542	0,097564	0,097564	-0,70573	24	0,1133	129,694573
9	1,618413	0,107056	0,107056	-0,7234	24	0,1108	135,9855339
10	1,692381	0,116858	0,116858	-0,74065	24	0,1085	142,2006211
11	1,765405	0,126946	0,126946	-0,75747	24	0,1064	148,3363897
12	1,837449	0,137293	0,137293	-0,77383	24	0,1046	154,3898148
13	1,908473	0,147873	0,147873	-0,78971	24	0,1028	160,3575354
14	1,978444	0,158658	0,158658	-0,80509	24	0,1013	166,2367787
15	2,047328	0,169619	0,169619	-0,81996	24	0,0998	172,0246879

Appendix B

Table B.1 – Aerofoil coordinates.

1.00000	0.00715	0.76280	0.09342	0.29573	0.14422
0.99984	0.00726	0.75313	0.09579	0.28601	0.14341
0.99939	0.00757	0.74335	0.09815	0.27643	0.14249
0.99867	0.00801	0.73347	0.10046	0.26698	0.14145
0.99761	0.00858	0.72346	0.10274	0.25764	0.14028
0.99622	0.00932	0.71332	0.10499	0.24841	0.13901
0.99456	0.01021	0.70308	0.10723	0.23933	0.13764
0.99263	0.01124	0.69277	0.10942	0.23039	0.13614
0.99040	0.01239	0.68235	0.11156	0.22158	0.13452
0.98787	0.01369	0.67183	0.11367	0.21289	0.13281
0.98509	0.01513	0.66124	0.11576	0.20435	0.13099
0.98208	0.01669	0.65058	0.11779	0.19597	0.12906
0.97880	0.01833	0.63985	0.11975	0.18773	0.12703
0.97524	0.02010	0.62904	0.12168	0.17962	0.12490
0.97146	0.02199	0.61818	0.12357	0.17167	0.12268
0.96747	0.02397	0.60728	0.12540	0.16389	0.12035
0.96324	0.02601	0.59633	0.12715	0.15625	0.11793
0.95876	0.02814	0.58532	0.12886	0.14876	0.11543
0.95407	0.03036	0.57429	0.13052	0.14143	0.11285
0.94919	0.03263	0.56325	0.13209	0.13429	0.11018
0.94410	0.03492	0.55218	0.13360	0.12729	0.10744
0.93877	0.03727	0.54107	0.13504	0.12046	0.10462
0.93326	0.03967	0.52997	0.13641	0.11380	0.10175
0.92756	0.04208	0.51888	0.13771	0.10732	0.09879
0.92164	0.04448	0.50779	0.13891	0.10101	0.09578
0.91549	0.04691	0.49668	0.14005	0.09486	0.09271
0.90916	0.04937	0.48561	0.14112	0.08889	0.08960
0.90264	0.05182	0.47457	0.14209	0.08312	0.08644
0.89591	0.05425	0.46355	0.14297	0.07752	0.08323
0.88895	0.05668	0.45254	0.14378	0.07208	0.07999
0.88179	0.05914	0.44160	0.14449	0.06685	0.07673
0.87445	0.06160	0.43071	0.14511	0.06180	0.07343
0.86691	0.06405	0.41986	0.14564	0.05694	0.07010
0.85915	0.06652	0.40905	0.14608	0.05226	0.06677
0.85122	0.06900	0.39833	0.14642	0.04777	0.06342
0.84313	0.07147	0.38769	0.14667	0.04349	0.06008
0.83485	0.07393	0.37710	0.14680	0.03939	0.05673
0.82638	0.07640	0.36659	0.14685	0.03548	0.05340
0.81775	0.07888	0.35617	0.14680	0.03177	0.05008
0.80898	0.08133	0.34586	0.14664	0.02826	0.04679
0.80004	0.08377	0.33563	0.14636	0.02496	0.04352
0.79093	0.08621	0.32548	0.14599	0.02184	0.04028
0.78169	0.08864	0.31545	0.14551	0.01892	0.03707
0.77232	0.09105	0.30554	0.14492	0.01622	0.03392
0.01372	0.03081	0.24736	-0.00173	0.91737	0.02816
0.01141	0.02774	0.25868	-0.00041	0.92628	0.02558
0.00932	0.02475	0.27015	0.00097	0.93467	0.02289
0.00744	0.02180	0.28179	0.00239	0.94253	0.02011
0.00577	0.01890	0.29357	0.00385	0.94982	0.01729

0.00429	0.01605
0.00303	0.01327
0.00200	0.01057
0.00118	0.00795
0.00056	0.00539
0.00016	0.00292
0.00000	0.00000
0.00007	-0.00169
0.00033	-0.00370
0.00083	-0.00554
0.00165	-0.00725
0.00284	-0.00879
0.00445	-0.01020
0.00645	-0.01150
0.00879	-0.01269
0.01143	-0.01375
0.01439	-0.01469
0.01767	-0.01554
0.02124	-0.01630
0.02511	-0.01696
0.02927	-0.01751
0.03375	-0.01797
0.03851	-0.01833
0.04356	-0.01860
0.04890	-0.01877
0.05455	-0.01885
0.06048	-0.01883
0.06670	-0.01872
0.07321	-0.01852
0.08002	-0.01822
0.08711	-0.01785
0.09449	-0.01740
0.10215	-0.01685
0.11009	-0.01623
0.11831	-0.01554
0.12679	-0.01479
0.13554	-0.01396
0.14457	-0.01306
0.15384	-0.01212
0.16334	-0.01113
0.17308	-0.01009
0.18307	-0.00898
0.19330	-0.00784
0.20373	-0.00668
0.21437	-0.00549
0.22520	-0.00427
0.23620	-0.00301
0.30551	0.00536
0.31761	0.00692
0.32986	0.00851
0.34226	0.01014
0.35480	0.01181
0.36748	0.01351
0.38031	0.01525
0.39327	0.01701
0.40638	0.01880
0.41965	0.02062
0.43309	0.02243
0.44667	0.02422
0.46037	0.02599
0.47419	0.02773
0.48814	0.02942
0.50217	0.03104
0.51628	0.03260
0.53044	0.03410
0.54467	0.03553
0.55893	0.03687
0.57320	0.03813
0.58748	0.03934
0.60178	0.04045
0.61607	0.04147
0.63031	0.04239
0.64452	0.04325
0.65871	0.04401
0.67285	0.04465
0.68691	0.04518
0.70090	0.04563
0.71483	0.04594
0.72867	0.04608
0.74235	0.04606
0.75585	0.04590
0.76917	0.04558
0.78225	0.04509
0.79505	0.04446
0.80759	0.04372
0.81987	0.04286
0.83189	0.04186
0.84362	0.04074
0.85508	0.03950
0.86630	0.03811
0.87724	0.03652
0.88783	0.03474
0.89807	0.03277
0.90795	0.03058
0.95652	0.01450
0.96266	0.01180
0.96829	0.00920
0.97337	0.00672
0.97790	0.00443
0.98196	0.00234
0.98558	0.00044
0.98873	-0.00125
0.99143	-0.00273
0.99374	-0.00396
0.99569	-0.00499
0.99725	-0.00584
0.99842	-0.00646
0.99926	-0.00686
0.99980	-0.00708
1.00000	-0.00715

Appendix C

C.1 - First Case

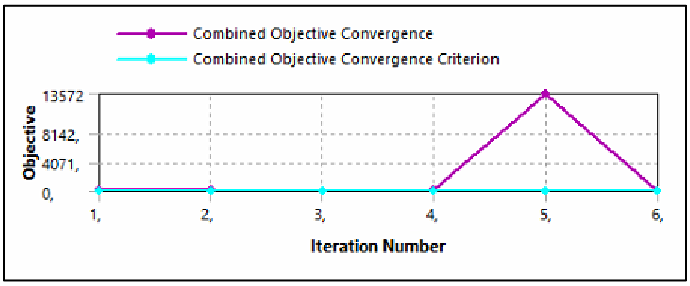

Figure C.1 – Objective convergence vs objective convergence criterion.

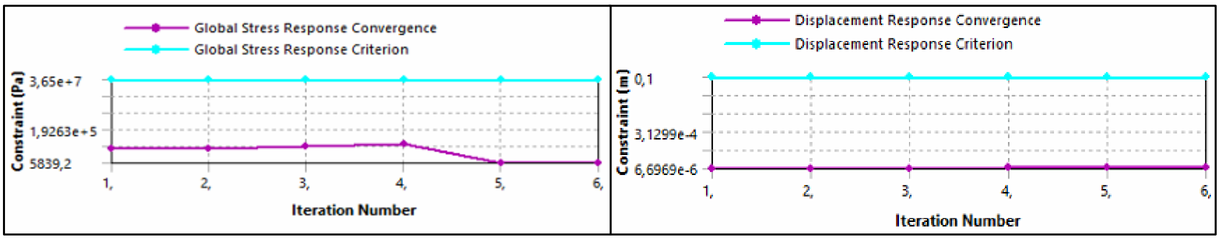

Figure C.2 – At left is presented the variation of global stress response and at right is the variation of displacement response.

C.2 - Second Case

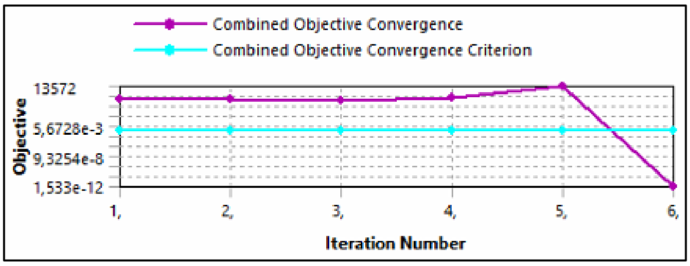

Figure C.3 – Objective convergence vs objective convergence criterion.

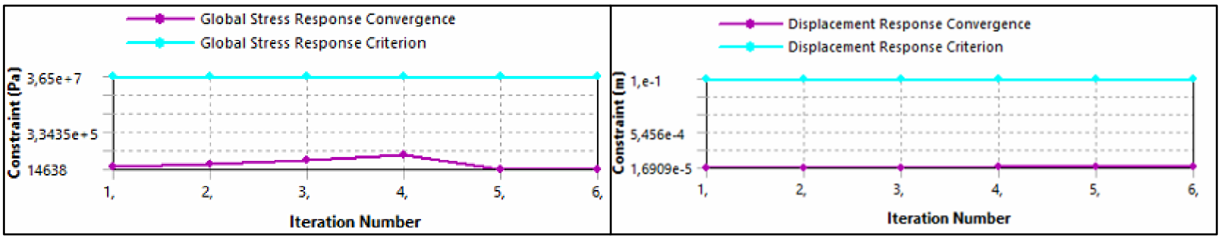

Figure C.4 – At left is presented the variation of global stress response and at right is the variation of displacement response.

C.3 – Third Case

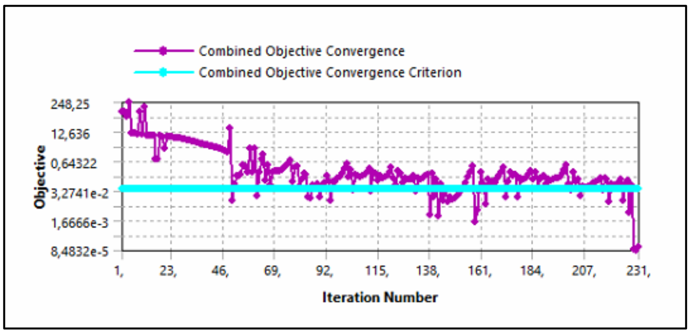

Figure C.5 – Objective convergence vs objective convergence criterion.

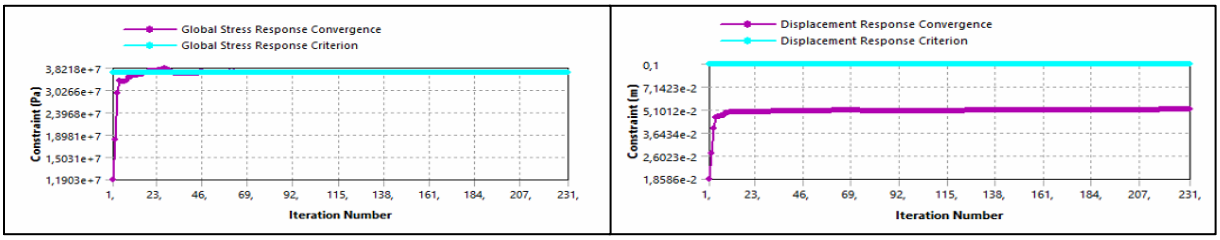

Figure C.6 - At left is presented the variation of global stress response and at right is the variation of displacement response.

Appendix D

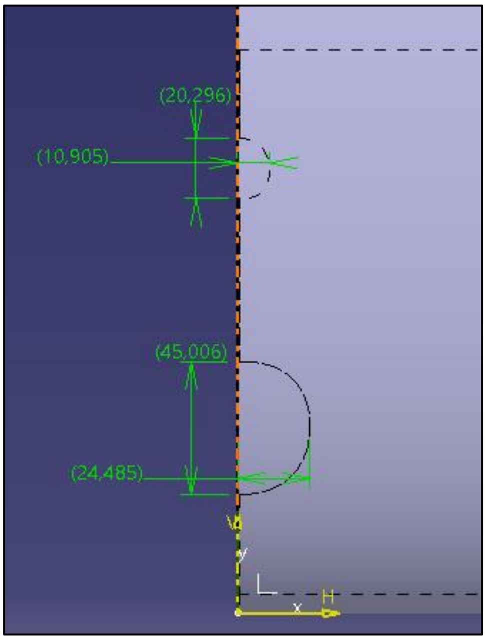

Figure D.1 – Dimensions from the support geometry of the connection between wing-fuselage.